Techniques and best practices in multiattribute display

Kurt J. Marfurt[1]

Abstract

All color monitors display images by mixing red, green, and blue (RGB) components. These RGB components can be defined mathematically in terms of hue, lightness, and saturation (HLS) components. A fourth alpha-blending (also called *opacity*) component provides a means to corender multiple images. Most, but not all, modern commercial interpretation workstation software vendors provide multiattribute display tools using an opacity model. A smaller subset of vendors provide tools to interactively display two or three attributes using HLS, CMY, and RGB color models. I evaluated a technique (or trick) to simulate the HLS color model using monochromatic color bars and only opacity. This same trick only approximates true color blending of RGB or CMY components. There are three basic objectives in choosing which attributes to display together. The first objective is to understand the correlation of one attribute to another, and most commonly, of a given attribute to the original seismic amplitude data. The second objective is to visualize the confidence or relevance of a given attribute by modulating it with a second attribute. The third objective is to provide a more integrated image of the seismic data volume by choosing attributes that are mathematically independent but correlated through the underlying geology. I developed the interpretation value of the HLS display technique on a 3D data volume acquired over the Central Basin Platform of west Texas exhibiting faults, fractures, folds, channels, pinch outs, and karst features. To be a useful "technique," I need to demonstrate these workflows within a specific package. Although I implemented the workflow in Petrel 2014, similar images can be generated using any software with flexible opacity capabilities. I also developed a short list of attribute combinations that are particularly amenable to corendering in HLS.

Preface

The vision for the new AAPG/SEG journal *Interpretation* introduced in 2013 was to be a scientific, peer-reviewed journal that would provide papers on best practices, algorithmic innovation, geologic calibration, effective interpretation workflows, and most important, integrated case studies for the modern geoscience interpreter. In addition to keeping abreast of such new developments, modern interpreters need to be aware of common pitfalls, the assumptions made in a given workflow, and techniques to achieve a given objective. For this reason, *Interpretation* has two regular sections for each issue. The first regular section is named "Pitfalls." Being more prone to pitfalls than other, more careful interpreters, I have coauthored two papers for this section. The second regular section is named "Tools, techniques, and tutorials." "Tutorials" form common contributions to GEOPHYSICS and *The Leading Edge*. "Tools" and "techniques" are less common, primarily because any given tool or technique may require describing it within a specific software package. Such endorsement of a given software package is against the AAPG and SEG publication and technical conference guidelines. Nevertheless, in now entering my 12th year of teaching an attribute course for these professional societies, the most common question I receive is "How do I do such-and-such in commercial package X?" In this paper, I will illustrate what I feel to be an effective multiattribute display technique using Schlumberger's Petrel 2014 product. Users of Landmark's DecisionSpace, Paradigm's VoxelGeo, TeraSpark's Insight Earth, and Foster Findlay's GeoTeric (and perhaps others) will note that these packages have an effective hue, lightness, and saturation (HLS) display built into them. I encourage this user community to respond with a follow on contribution to show effective multiattribute interpretation techniques using these packages. Ideally, the result will be a more informed and skilled interpretation community.

Introduction

A good attribute quantifies a geometric, kinematic, dynamic, or statistical property of the seismic amplitude data (Liner et al., 2004). Combinations of multiple attributes should be mathematically independent but somehow coupled through the underlying geology

[1]University of Oklahoma, College of Earth and Energy, Norman, Oklahoma, USA. E-mail: kmarfurt@ou.edu.

Manuscript received by the Editor 1 July 2014; revised manuscript received 29 August 2014; published online 21 January 2015. This paper appears in *Interpretation*, Vol. 3, No. 1 (February 2015); p. B1–B23, 25 FIGS., 2 TABLES.

http://dx.doi.org/10.1190/INT-2014-0133.1.

(Barnes, 2007). Because good seismic attributes represent key aspects of the underlying geology, corendering more than one attribute in the same image may provide increased geologic insight.

There are three-color models — the red-green-blue (RGB) color model used in mixing light such as on a television screen or computer monitor, the cyan-magenta-yellow-black (CMYK) color model used in printing and painting, and the hue-lightness-saturation (HLS) model that is mathematical in nature but provides a means of modulation of one attribute by another. The hue-saturation-value (HSV) color model is an alternative representation of the HLS model. A careful description of the differences between HLS and HSV space can be found in Joblove and Greenberg (1978). Although this paper addresses color blending, most commercial software also provides a means of combining attributes using shaded relief (Barnes, 2002) and bump map (Lynch et al., 2005) constructs.

The practical limitation to multiattribute display is a function of the number of colors available (Dao and Marfurt, 2011). Several commercial interpretation software packages now provide 24-bit (>16 million) color with 8-bit (256) color for each of the RGB display components. Such color depth is routinely provided in the free software that comes with your digital camera. Although such "true color" was simulated in earlier cathode-ray tube and liquid-crystal display monitors, the OpenGL software standard and most monitors today support 256^3 colors. Introducing such color depth to commercial software with a historical user base is extremely difficult because color display forms the foundation of seismic interpretation. For this reason, many commercial interpretation software packages are currently limited to 256 colors per image.

Knoblock (1982) is perhaps the earliest user of the HLS color model to display seismic attributes, mapping instantaneous phase against a cyclical polychromatic hue color bar and instantaneous envelope against lightness. Zones of anomalously low envelope appear as a background black, gray, or white color. In one of the first tutorial papers on 3D seismic interpretations, Rijks and Jauffred (1991) show how one could effectively corender dip azimuth (against hue) and dip magnitude (against lightness). The azimuths at zero dip magnitude are displayed as a background white color. Marfurt et al. (1998) use the same HLS color model to corender dip-azimuth (against hue), dip magnitude (against saturation), and coherence (against lightness). Guo et al. (2010, 2012) show how one can modulate the strike of curvature (against hue) by its magnitude (against saturation or lightness) providing a continuous (one voxel resolution) display.

Azimuthal anisotropy is commonly displayed as icons, with the direction of a bar or arrow aligned with the strike of maximum anisotropy, the color of the bar or arrow defined by the degree of anisotropy, and the length of the bar or arrow by the magnitude of the larger velocity or azimuth gradient. A limitation of this display technique is that each icon is 5–10 voxels in size, thereby limiting either the size or the resolution of the display on a fixed-sized monitor. Guo et al. (2008) and Zhang et al. (2013) use HLS to corender the strike of azimuthal anisotropy (against hue) by its magnitude (against saturation or lightness). Zhang et al. (2013) then use the lightness axis to corender corresponding images of confidence in the azimuthal computation, coherence, or curvature, the latter showing an apparent compartmentalization of hydraulic fracturing. Hypothesizing that there may be structural control on azimuthal anisotropy Guo et al. (2013) crosscorrelate the vector (strike and magnitude) structural deformation with the vector (strike and magnitude) azimuthal anisotropy, resulting in a vector correlation coefficient. Each

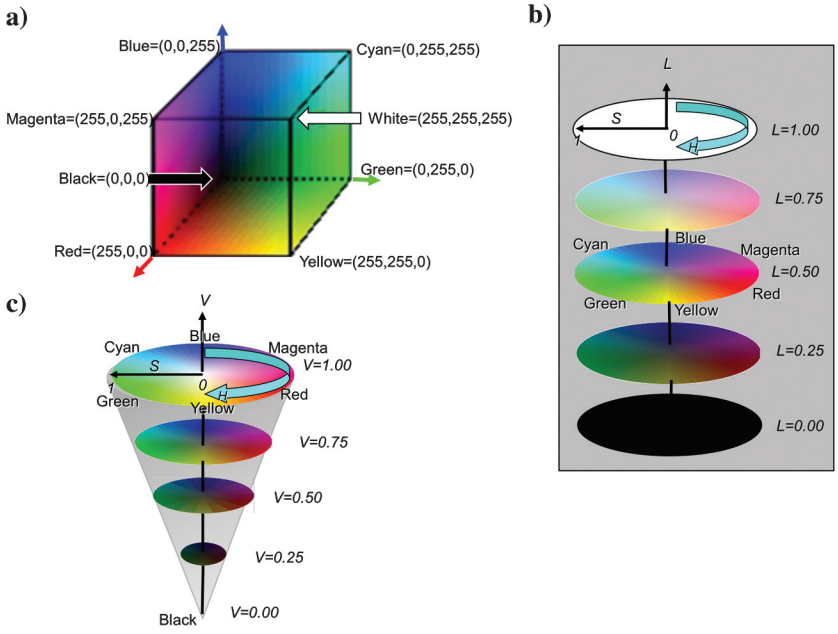

Figure 1. (a) The RGB color cube showing its relation to the CMYK color model. The R, G, and B axes can be thought to be components of a color vector. (b) The HLS color model mapped to cylindrical coordinates. Hue has the range $0° < H < 360°$ and is mapped against the azimuth, lightness has the range $0.0 < L < 1.0$ and is mapped to the vertical axis, and saturation has the range $0.0 < S < 1.0$ and is mapped to radius. Foley and van Dam (1982) define blue to be 0°, but software vendors often set red or green to be 0°. (c) The HSV color model displayed as a cone. Hue and saturation have identical ranges and definitions to that of the HLS model. In contrast, value has the range $0.0 < V < 1.0$ and is mapped to the vertical axis. A value of $V = 0.0$ for any H or S corresponds to black, The triplets (H, $V = 1.0$, $S = 1.0$) correspond to pure colors, whereas the pair $V = 1.0$, $S = 0.0$ for any H corresponds to white.

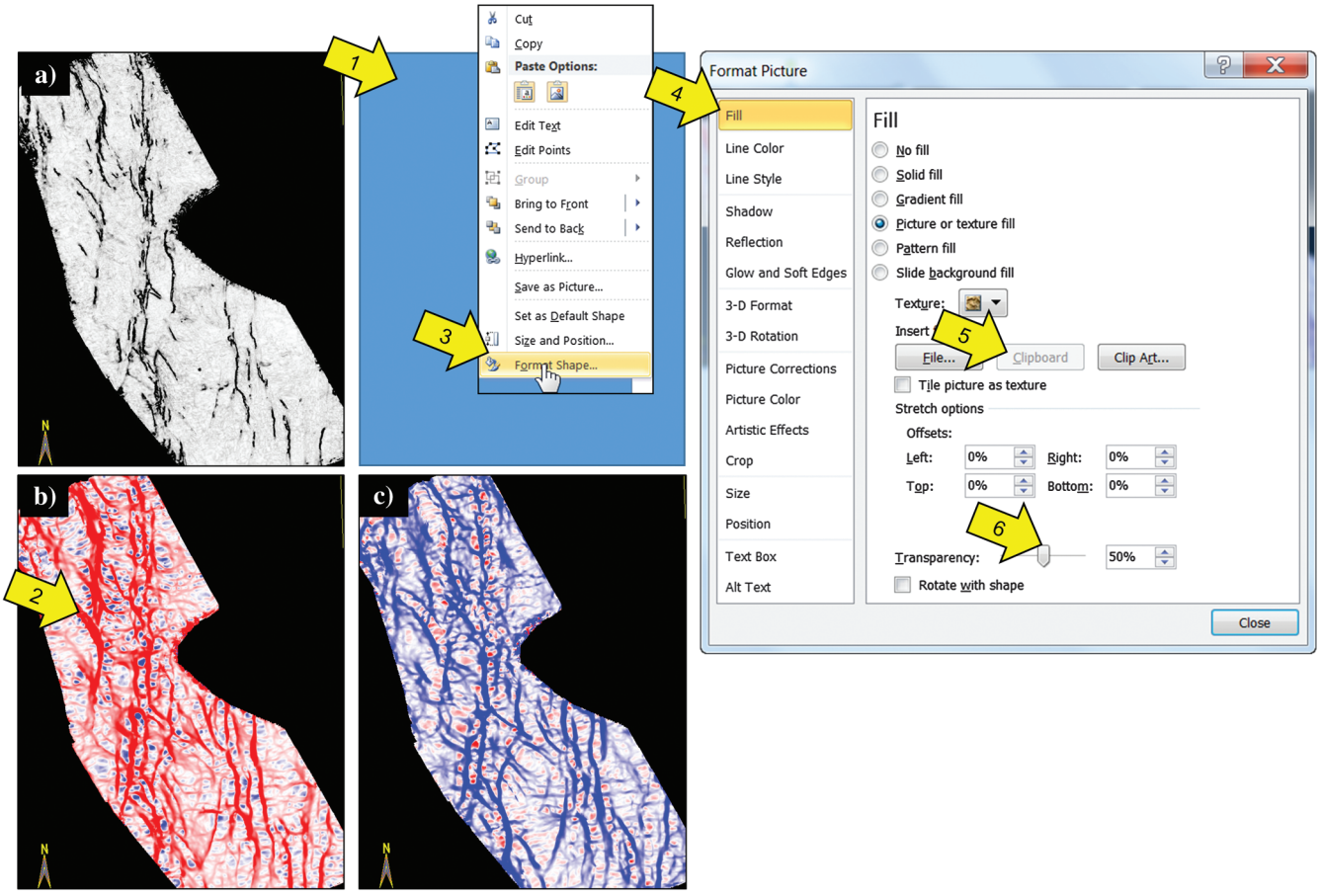

Figure 2. Using transparency to blend previously published images (Chopra and Marfurt, 2007) in PowerPoint: (a) coherence, (b) most-positive curvature, and (c) most-negative curvature. (1) Construct a box of the desired size. (2) Copy the desired image to overlay onto the clipboard. (3) Right-click the previously defined blue box and select "format shape." (4) Select "fill" in the pop-up menu. (5) Select the image to use in the fill, in this case, the image on the clipboard. (6) Slide the transparency bar to the desired level (in this example 50%). Repeat the process for the most-negative curvature image.

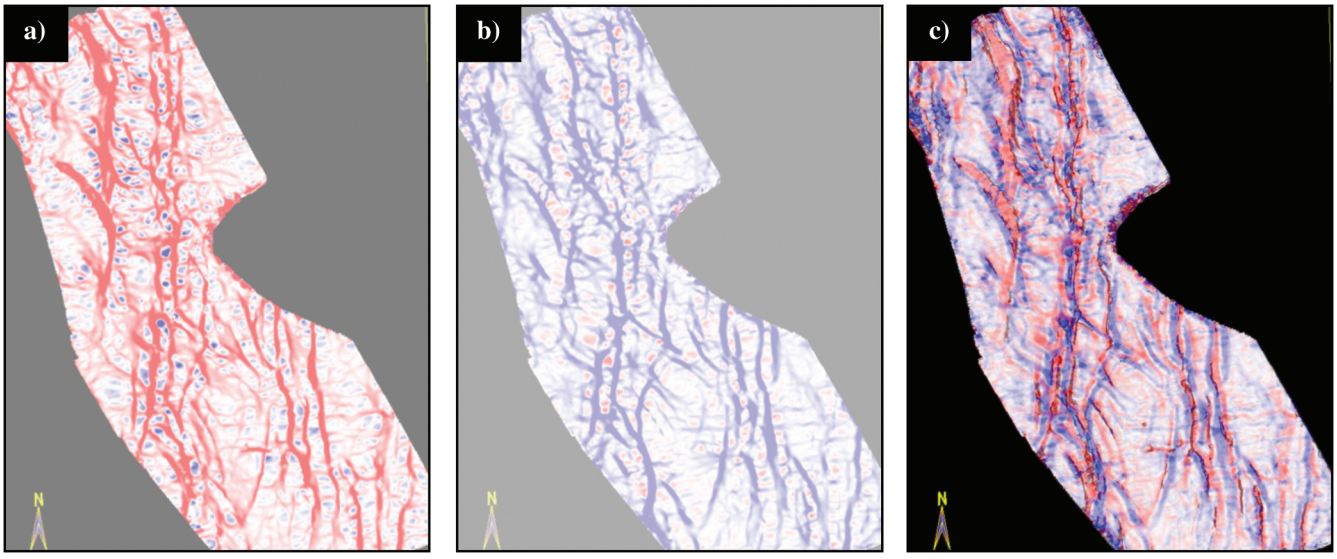

Figure 3. The (a) most-positive and (b) most-negative transparency images plotted using equation 3 with α=50% and β=33%plotted with 56% transparency. Note that the black background is now gray because we see through the image into the white background. (c) Corendered coherence, most-positive curvature, and most-negative curvature obtained by aligning panels (a) and (b) with the coherence image shown in Figure 1a. Coherence anomalies bracketing positive (red) curvature anomalies indicate horsts, and coherence anomalies bracketing negative (blue) curvature anomalies indicate grabens.

three of these values can be readily displayed using an HLS color model.

Angular unconformities and depositional clinoforms are also described by azimuth and magnitude. Masaferro et al. (2003) first flatten on an underlying reference horizon prior to computing volumetric dip azimuth and dip magnitude. This latter measurement, displayed against hue and lightness, provided a spatial view of the carbonate shoal pinch outs. Marfurt and Rich (2010) and Marfurt (2010) find that two of the components of the mathematical curl of vector dip provide a volumetric estimate of reflector convergence, removing the need to flatten on a horizon.

Modern RGB display of spectral attributes is envisioned by Balch (1971). Onstott et al. (1984), use RGB to corender near-, mid-, and far-offset amplitude data. Today, three spectral components are routinely plotted against RGB. An alternative to choosing the "best" three components is to corender the peak frequency (plotted against hue) and the peak magnitude (plotted against lightness or saturation) (Liu and Marfurt, 2007a, 2007b; Guo et al., 2008). More recently, Purves, and Basford (2011) show how three attributes can be combined against CMY to provide enhanced images of faults and fault damage zones.

In this paper, I show how one can simulate the HLS model by using monochrome black, white, and gray color bars and an opacity tool. I begin with a simple overview of the RGB, CMYK, HLS, and alpha-blending color models. I then introduce what I consider to be a "presentation survivor skill" by showing how one can blend three previously published images in Microsoft PowerPoint2010. I further illustrate the linkage between opacity and the HLS color model using a simple polychromatic color bar and a monochrome gray and a binary black and white color bar using the same PowerPoint tool. I then move to color display of attributes in the commercial workstation environment, showing how one needs to turn off the defaults in the display of cyclical data for all interpretation workstation software that I have used. The variance and dip azimuth and dip magnitude volumes, and all displays are made in Petrel 2014. Other attributes were generated using software developed at the University of Oklahoma and loaded into Petrel 2014 for display and subsequent interpretation. The key objective is to illustrate the effectiveness of HLS display in corendering a variety of seismic attributes. I conclude by showing that the opacity strategy does not provide the desired color addition (subtraction) in corendered RGB (CMYK) images.

Methodology

Red-green-blue; cyan-magenta-yellow; hue, lightness, and saturation; and alpha blending

Traditionally, the computer monitor is displayed using three colored phosphors or lamps — red, green, and blue. As a geophysicist, it is natural to think of a given image as having three (R, G, and B) components. Color display is then the (optical) addition of the R, G, and B components. Figure 1a shows the RGB color model. Notice that it is easy to convert from RGB to CMYK to print a color image as a hardcopy. Most values of R, G, and B will range between zero and 255 (implying a limit of 256 or 8-bit color along each axis), but one will also encounter ranges from 0.0 to 1.0 and 0.0 to 100.0.

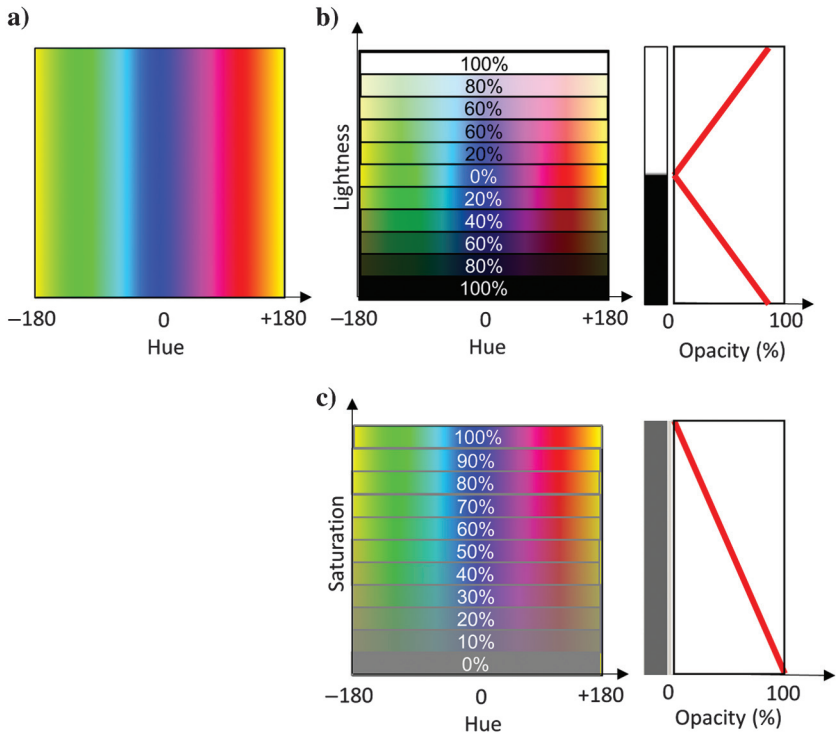

Figure 4. (a) The cyclical hue color bar defined with yellow = ±180°, green = −120°, cyan = −60°, blue = 0°, magenta = +60°, and red = +120°. (b) Hue versus lightness plotted using PowerPoint. In this image, I took the azimuth color bar and overplotted it with six black bars and five white bars of variable transparency indicated as shown. (c) Hue versus saturation using PowerPoint. In this image the azimuth color bar is overplotted with 11 monochromatic gray color bars of variable transparency.

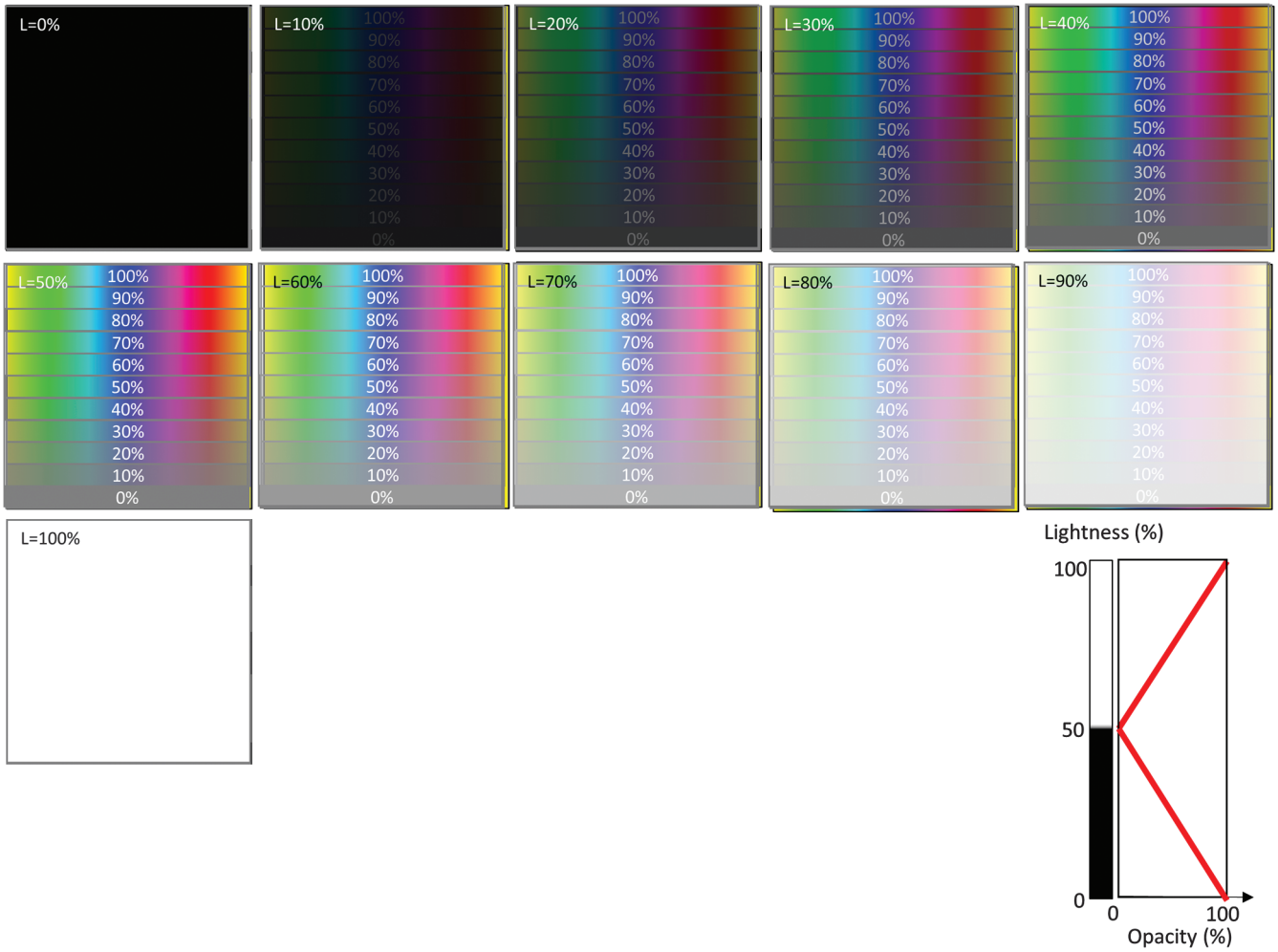

Figure 5. Hue versus saturation versus lightness using PowerPoint. Each image is a constant lightness slice. To simulate lightness, the image in Figure 4c is overlain by either a white or a black box using the binary color bar and opacity shown in the image to the lower right. Note that for L = 0%, the overlay is a completely opaque black box, for L = 50% it is a completely transparent box, and for L = 100% it is a completely opaque white box.

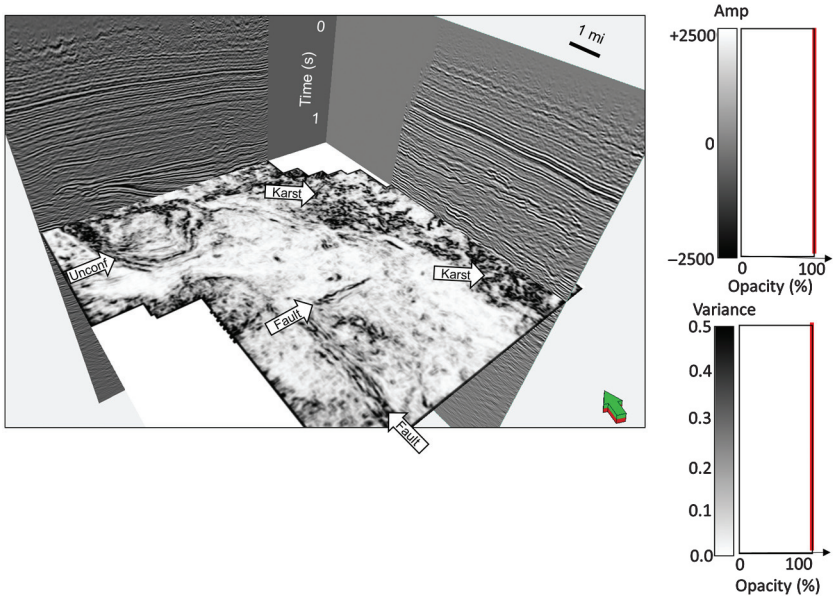

Figure 6. A traditional seismic display showing seismic amplitude on the vertical slices and a time slice at $t = 1.226$ s through variance. Correlation of the variance attribute is done through animation of the two vertical slices against the time slice.

The HLS color model shown in Figure 1b is a modified version of Foley and van Dam's (1982) double pyramid, where the cyclical hue axis assigns a value of 0° to blue. Many implementations will set saturation and lightness to vary between 0.0 and 1.0, or 0.0 and 100.0, whereas the one I use here (Petrel) varies between zero and 240. Likewise, many implementations will have hue variation between zero and 360 or −180 and +180, indicating the periodicity of the color bar. Petrel's varies between zero and 240 (Appendix A). I suspect the 240 is a holdover of earlier software implementations in which 16 colors were reserved for seismic picks and annotation and 240 for color display (giving a total of 256). This was the case for earlier versions of GeoFrame's IESX and Landmark's OpenWorks, and it remains this way for Kingdom Suite.

If we wish to corender two images (such as the gray-scale seismic display and green fault plane described by Meyer et al., 2001), we need to average the RGB components of each image. Let us assume we have three different attributes: **a**, **b**, and **c**, each of which is represented by its RGB components:

$$\mathbf{a} = \begin{pmatrix} a_R \\ a_G \\ a_B \end{pmatrix}, \quad \mathbf{b} = \begin{pmatrix} b_R \\ b_G \\ b_B \end{pmatrix}, \quad \text{and} \quad \mathbf{c} = \begin{pmatrix} c_R \\ c_G \\ c_B \end{pmatrix}. \quad (1)$$

Corendering attributes **a** and **b** to obtain **f** is then obtained by applying opacity α to the second image **b**:

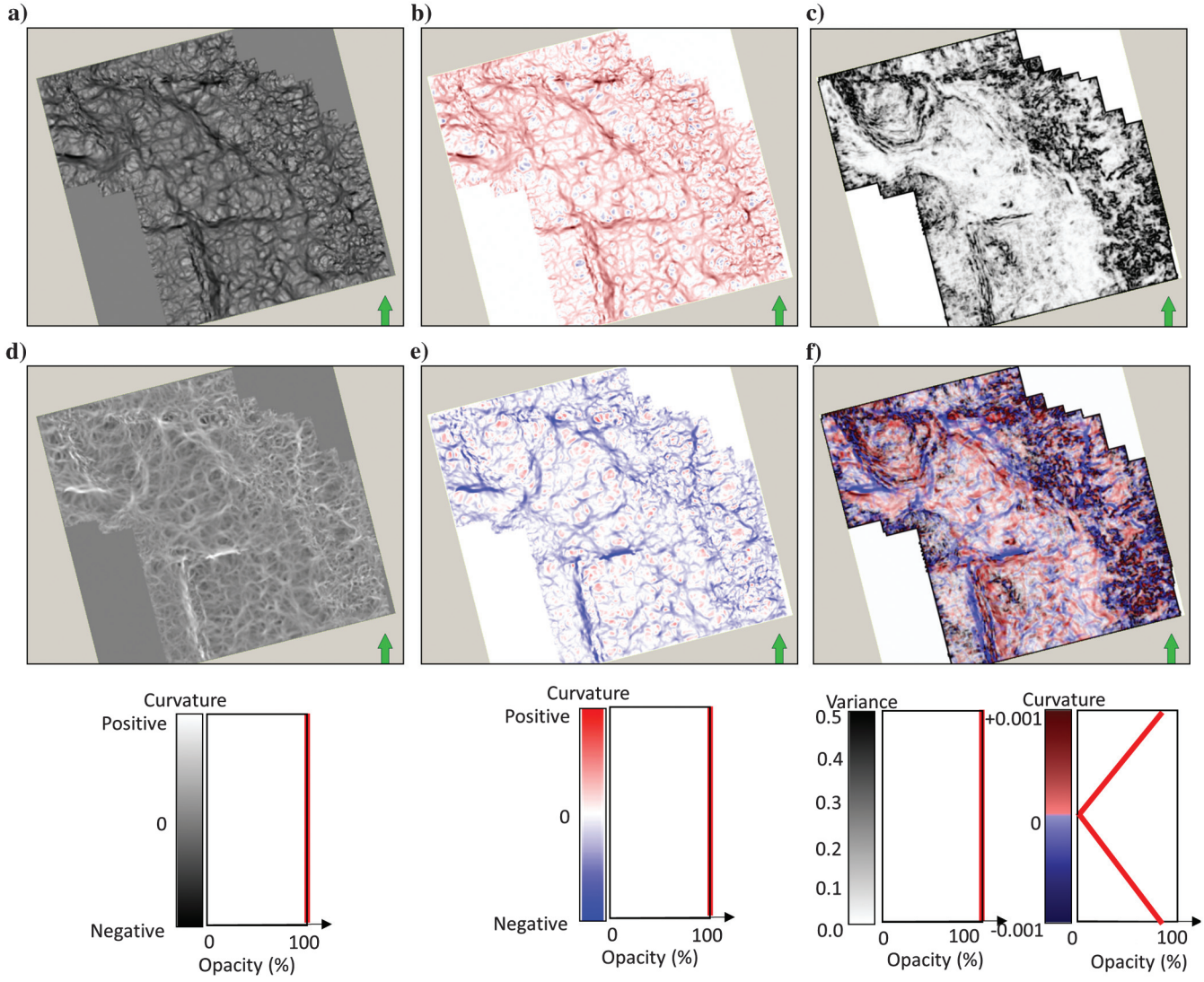

Figure 7. Time slices at $t = 1.226$ s through most-positive curvature, k_1, using a (a) gray scale and (b) red-white-blue color bar, and most-negative curvature, k_2, using a (d) gray scale and (e) red-white-blue color bar. As discussed in Brown (2011) the human eye sees edges much better in monochrome as in panel (a) than in the polychromatic color shown in panel (b). Mapping of (negative) anomalies against white in panel (d) gives the impression of a negative of a photograph, and it is somewhat "artificial," although such images appear in nature such as caustics of sunlight on the bottom of a swimming pool with waves on the surface. (c) Variance plotted against gray scale. (f) Corendering of the polychromatic images in panels (b) and (e) with the gray-scale variance in panel (c). Corendering of panels (a and d) with each other or with panel (c) provides inferior images.

$$\begin{pmatrix} f_R \\ f_G \\ f_B \end{pmatrix} = (1-\alpha)\begin{pmatrix} a_R \\ a_G \\ a_B \end{pmatrix} + \alpha\begin{pmatrix} b_R \\ b_G \\ b_B \end{pmatrix}. \quad (2)$$

Corendering the resulting blended image, **f**, with attribute **c** is obtained by applying opacity β to **c**:

$$\begin{aligned}\begin{pmatrix} g_R \\ g_G \\ g_B \end{pmatrix} &= (1-\beta)\begin{pmatrix} f_R \\ f_G \\ f_B \end{pmatrix} + \beta\begin{pmatrix} c_R \\ c_G \\ c_B \end{pmatrix} \\ &= (1-\beta)(1-\alpha)\begin{pmatrix} a_R \\ a_G \\ a_B \end{pmatrix} + (1-\beta)\alpha\begin{pmatrix} b_R \\ b_G \\ b_B \end{pmatrix} \\ &\quad + \beta\begin{pmatrix} c_R \\ c_G \\ c_B \end{pmatrix}. \quad (3)\end{aligned}$$

The variable α used in equation 2 gives rise to the name *alpha blending*. If attribute **a** forms the background image, then α applied to the foreground image is called *opacity* and $(1-\alpha)$ is called *transparency*. Thus, if $\alpha = 0.0$, attribute **b** is 100% transparent and all we see is attribute **b**. Conversely, if $\alpha = 1.0$, attribute **b** is 0% transparent (or opaque) and it hides the image of attribute **a** such that all we see is attribute **b**.

Blending in PowerPoint2010

Often, we find an image in a published paper that we wish to manipulate after it has been published. This may occur even for the original author because he or she may no longer have access to the original data. Figure 2a–2c was previously published in a paper by Chopra and Marfurt (2007). Let us use PowerPoint to corender it following the instructions in the caption. You should be able to generate the two intermediate images in Figure 3a and 3b and merge them with Figure 2a to generate Figure 3c. The transparency values in the PowerPoint color bar are $(1-\alpha)$ and $(1-\beta)$ in equation 3. If we wish to have all three images appear with the same 1/3 contribution, some simple arithmetic will show that one should set $\alpha = 1/2$ *and* $\beta = 1/3$.

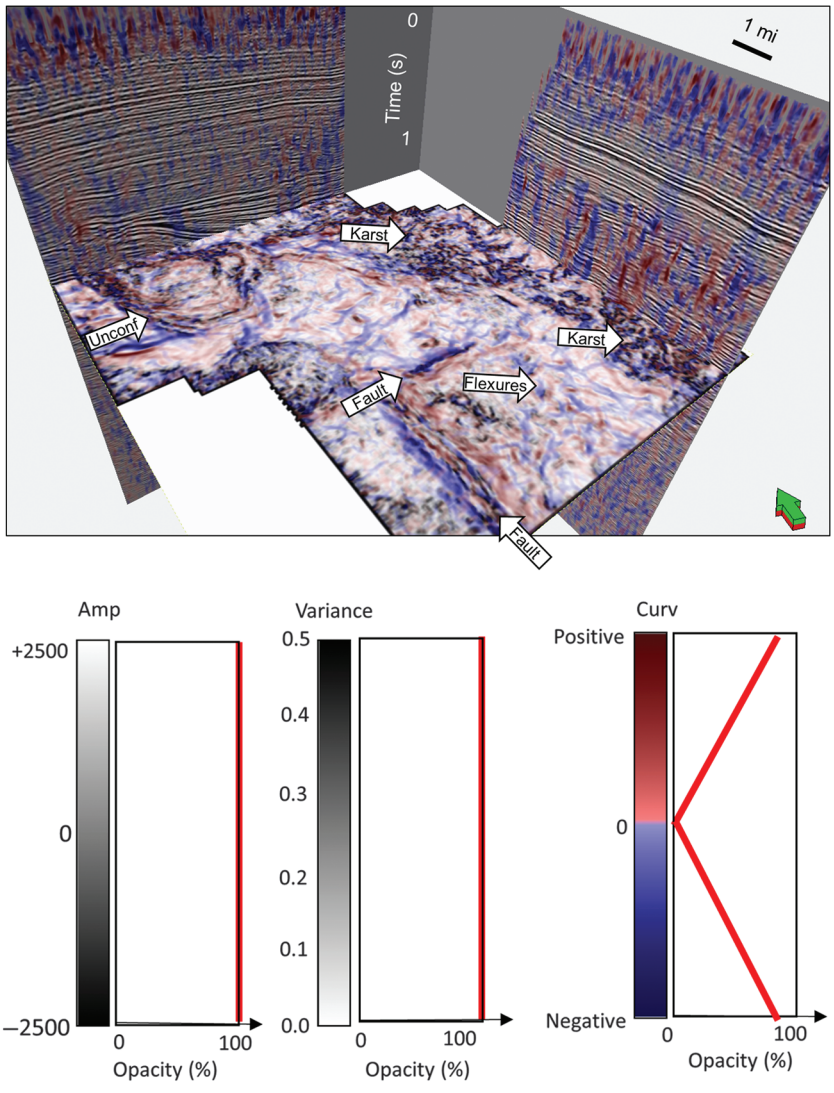

Figure 8. The same slices shown in Figure 6 but now corendered with most-positive and most-negative principal curvatures, k_1 and k_2. Geologic interpretation of these attributes is made by correlating them to the more traditional vertical slices through seismic amplitude and the time slice through variance. Note that on the vertical slices, positive curvature anomalies in red correlate to anticlinal features whereas negative curvature anomalies in blue correlate to synclinal features. Positive and negative curvature anomalies also bracket the variance anomalies seen along faults on the time slice, with positive curvature on the upthrown block and negative curvature on the downthrown block.

Simulating hue, lightness, and saturation in PowerPoint

Although Figure 1b summarizes the HLS color model, we can gain further comfort, if not insight, by building one in PowerPoint. In this example, I will use a simple cyclical color bar as my background. Note that I have mapped 0° to blue and $+180^{\circ}$ and -180° against yellow. The construction of such a color bar is available in all commercial workstations. I show in Appendix A how to accomplish this in Petrel.

To construct an HL (S = 100%) color bar, I define 11 boxes that are the same width but 1/11th the height of the hue color bar. Figure 4b shows the same binary black and white color bar. The value printed in each box is the value of the opacity (1-transparency) set in PowerPoint. Note that for the center box, the opacity = 0% and thus is completely transparent. Note how the colors progress from black to "midnight" colors to pure colors to "pastel" colors to white. Mathematically, we are blending either a white vector **w**

$$\mathbf{h} = (1-\alpha)\mathbf{a} + \alpha\mathbf{w} = (1-\alpha)\begin{pmatrix} a_R \\ a_G \\ a_B \end{pmatrix} + \alpha\begin{pmatrix} 1 \\ 1 \\ 1 \end{pmatrix}, \quad (4)$$

or a black vector $\mathbf{k} = (\mathbf{1}-\mathbf{w})$

$$\mathbf{h} = (1-\alpha)\mathbf{a} + \alpha\mathbf{k} = (1-\alpha)\begin{pmatrix} a_R \\ a_G \\ a_B \end{pmatrix} + \alpha\begin{pmatrix} 0 \\ 0 \\ 0 \end{pmatrix}, \quad (5)$$

with image **a**.

The hue-saturation (HS) color bar with lightness = 50%, shown in Figure 4c is slightly simpler. Here, I set the opacity of a monochrome gray color bar to range from 100% (no saturation) to 0% (pure colors).

The final step is to combine the HL and HS transparency workflow together. I use Figure 4c (the saturation modulated cyclical color bar) as my background image, and then I construct a suite of 11 squares to overlay it. The squares use the binary black and white color bar and the bilinear transparency definition, which gives me Figure 5.

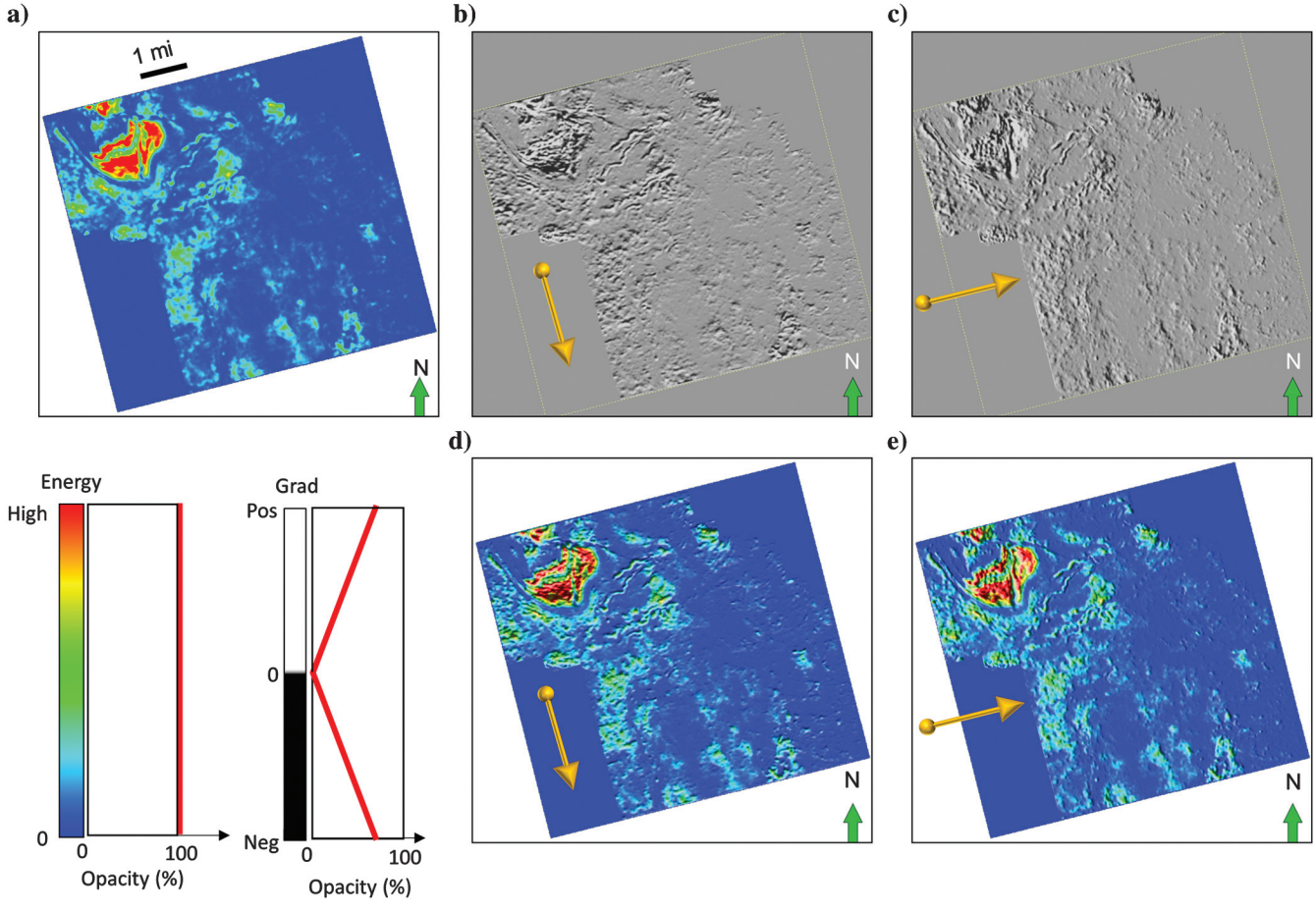

Figure 9. Time slices at $t = 1.060$ s through (a) coherent energy computed in a 9-trace × 20 ms window plotted against a polychromatic color bar, and (b) inline energy gradient and (c) crossline energy gradient plotted against a binary black and white color bar using transparency against a gray background. Panels (b) and (c) are then corendered with panel (a) to generate panels (d and e), giving the appearance of a shaded relief map of energy on a time slice. Orange arrows indicate the direction of the gradient.

Application

The data shown in Figure 6, acquired in the late 1990s by Burlington Resources over the Central Basin Platform of west Texas, have been discussed in several papers. Marfurt and Rich (2010) discuss attributes to map unconformities, whereas Liu and Marfurt (2007a) use spectral components to illuminate channels draining theses unconformities. Dou et al. (2009) describe karst and cave collapse visible on the east side of the time slice, and Fu et al. (2006) describe spiculitic chert and fractures seen on the western part of the time slice. I consider Figure 6 to be a conventional seismic interpretation image, with amplitude plotted against a gray scale to emphasize pinch outs and faults. Variance (which is $1.0 - c$, where c is coherence) is plotted on a time slice through the top of the Thirty-One spiculitic chert reservoir.

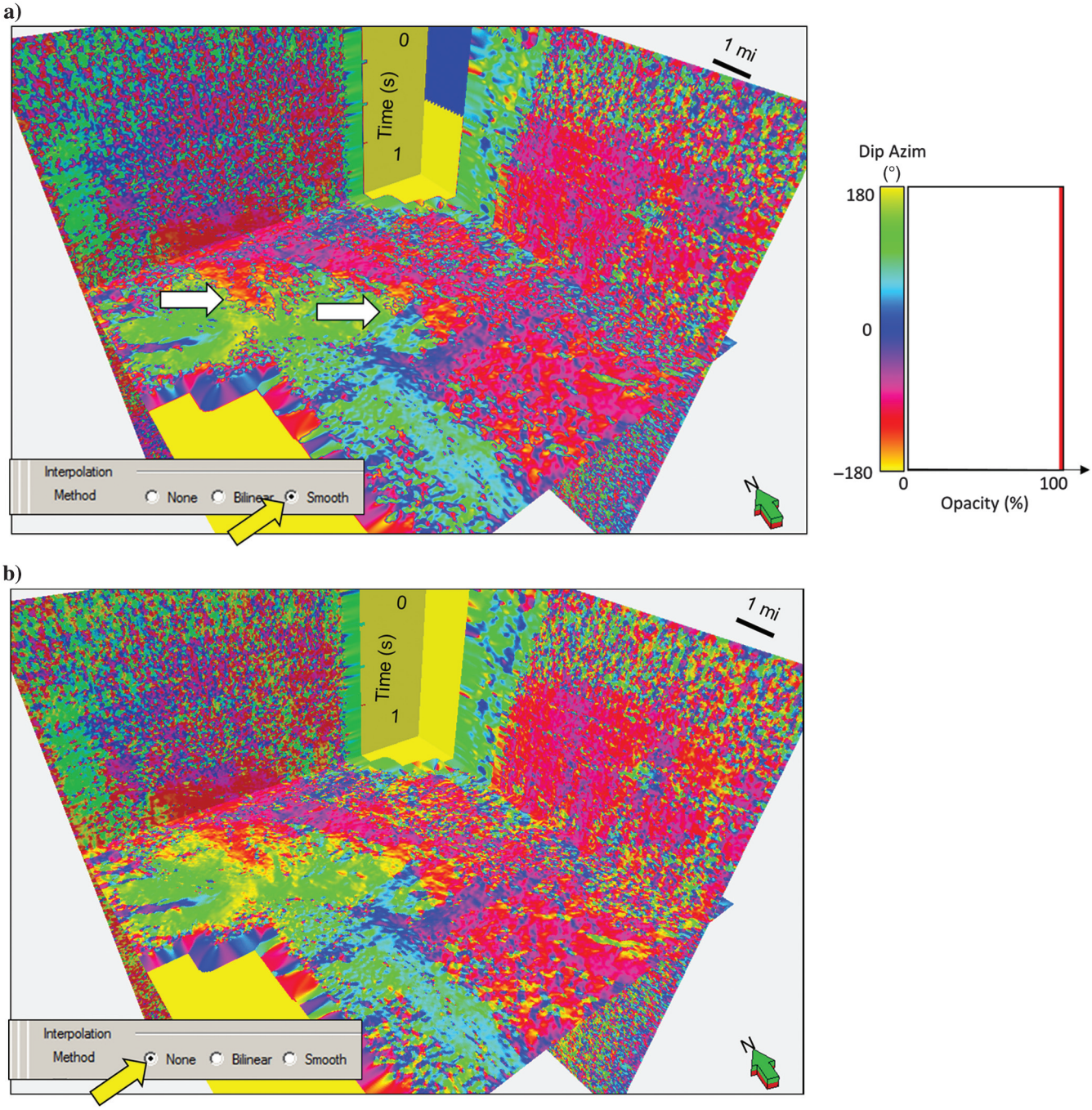

Figure 10. Vertical slices and a time slice at $t = 1.226$ s through a dip azimuth volume using (a) the default smooth interpolation and (b) no interpolation or "none" as indicated by the yellow arrow in Petrel's "settings" tab. With smooth interpolation turned on, voxels that have neighbors near -180° on one side and near $+180^\circ$ on the other side (both of which map to yellow) have interpolated values near 0° giving rise to the blue-stripe artifacts (indicated by white arrows). By selecting "none," interpolation is turned off and the otherwise empty voxels are assigned to the value of their nearest neighbor, removing the artifacts.

Simple corendering of curvature and amplitude

In Figure 7, I show the same time slice in a 2D view through most-negative and most-positive principal curvature, through variance, and through a corendered version of all three. In his classic book on 3D seismic interpretation, Alistair Brown (2011) recommends the use of monochrome when looking for edges, and polychrome when we wish to detect nonedge (e.g., amplitude) anomalies. For this reason, I show the curvature images using two color bars. The lineaments (or "edges") show up much better in monochrome gray scale in Figure 7a and 7d, but they will have limited use in blending with each other or with coherence if they all use the same color bar. A common way to corender curvature with seismic amplitude is to use a red-white-blue (or other dual-gradational color bar, see Brown, 2011) with either fixed 50% opacity or opacity that goes to zero for curvature values close to zero. Instead of a dual-gradational color bar, I use a bimodal color bar and opacity that provides better color and hence attribute fidelity. Examining the color legend for curvature, note that it is red for positive values and blue for negative values. I set the transparency value to be 0.0 at curvature values of 0.0 (denoting a plane) and ramp it linearly to the minimum and maximum curvature values. Unlike the more commonly used red-white-blue color bar, the "color" white never blends in with the underlying images, generating the clear image seen in Figure 7f.

In Figure 8, I now use this curvature color bar to overlay the most-positive and most-negative principal

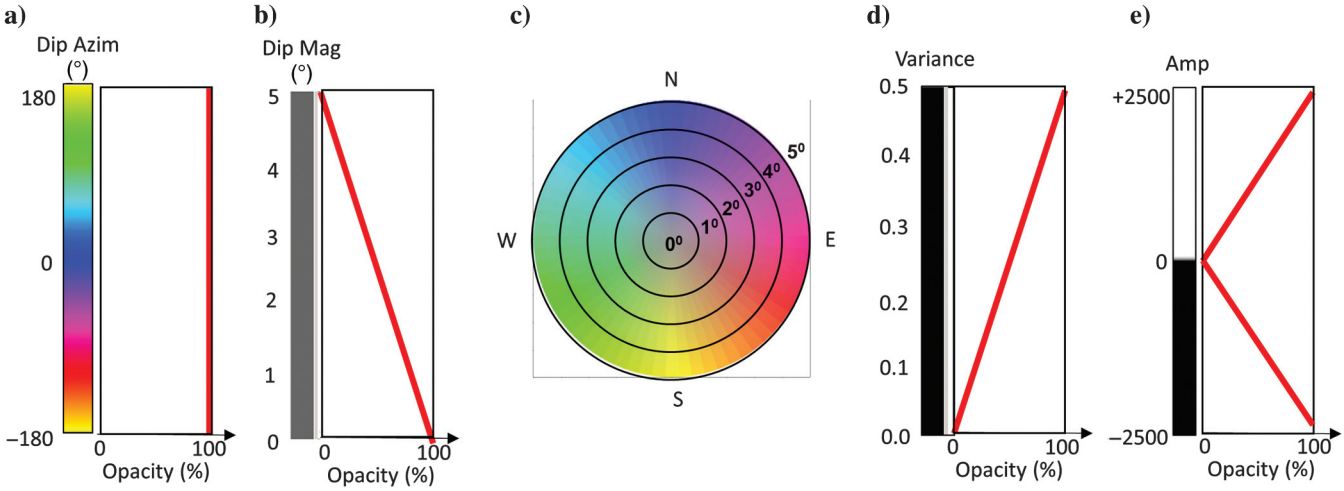

Figure 11. A suite of 1D color bars that with attribute corendering can simulate 2D and 3D color bars. (a) A cyclical color bar used to display dip azimuth forms the background image with opacity = 100%. (b) A monochromatic gray color bar that with corendering maps dip magnitude against saturation. Together, these two 1D color bars simulate (c) the 2D HS color wheel. Note that all dip azimuths have the same gray color at dip magnitude = 0°. (d) A monochromatic black color bar that with corendering maps variance against lightness. (e) A binary black-and-white color bar that with corendering maps positive amplitudes to white and negative amplitudes to black proportional to the amplitude value.

Figure 12. The same image shown in the previous figure but now corendered with dip magnitude plotted against the saturation color bar shown in Figure 11b. Flatter dips now appear more muted, whereas steeper dips appear as pure colors.

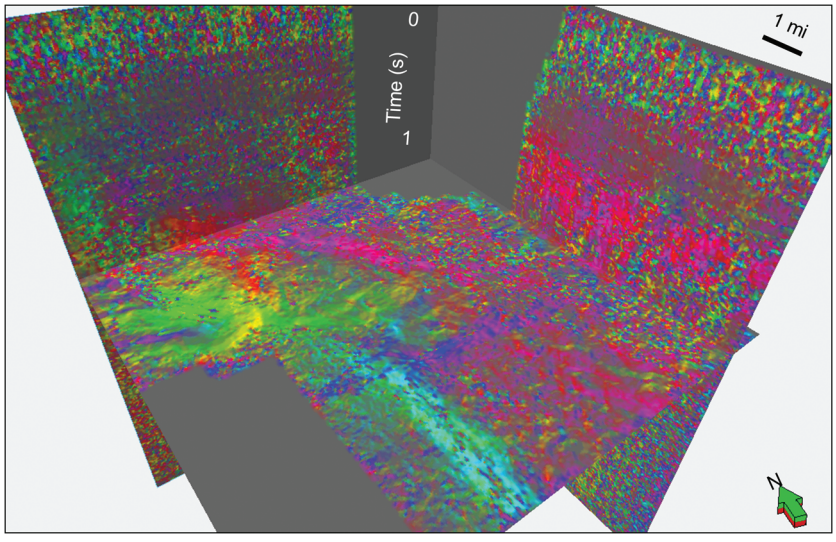

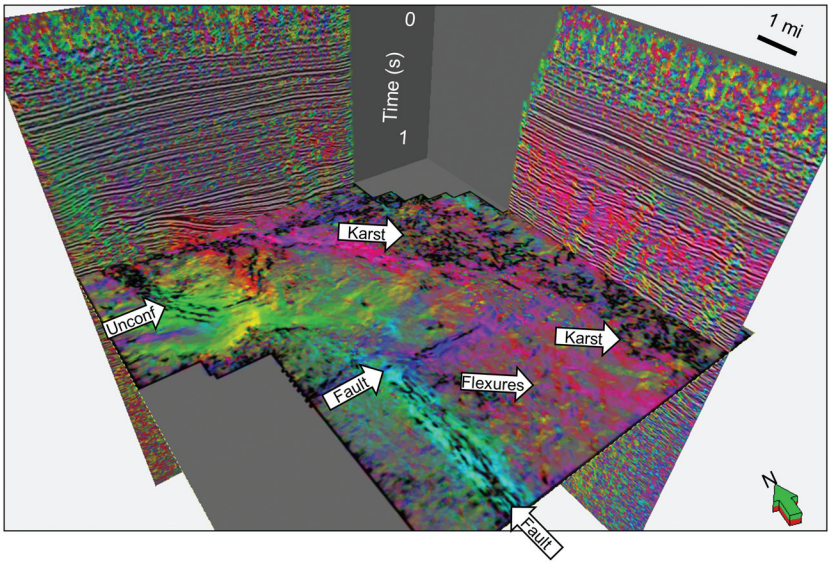

Figure 13. The same image shown in the previous figure but now corendered with variance plotted against the lightness color bar shown in Figure 11d. Variance delineates a north–south-trending reverse fault on the west, an east–west-trending strike-slip fault in the middle, an angular unconformity in the northwest, and karst features to the east. The flexures in the center fault block were previously delineated by curvature in Figure 8.

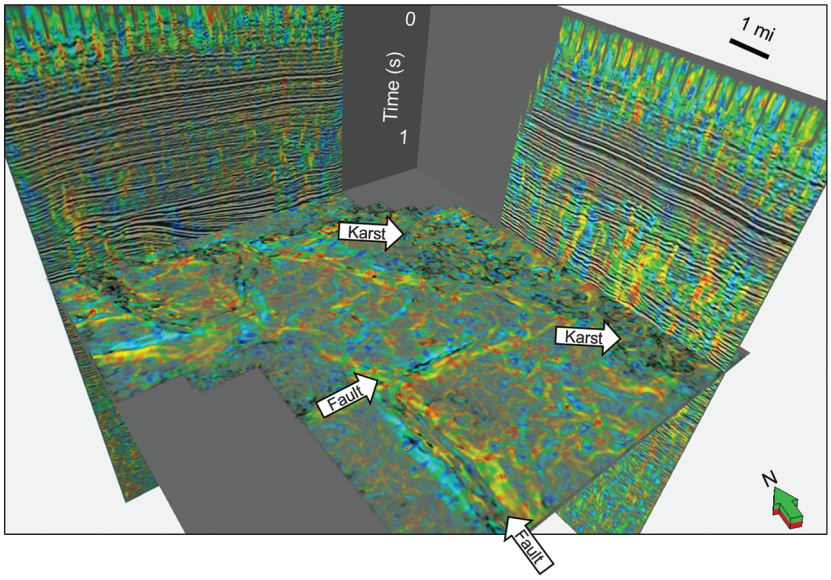

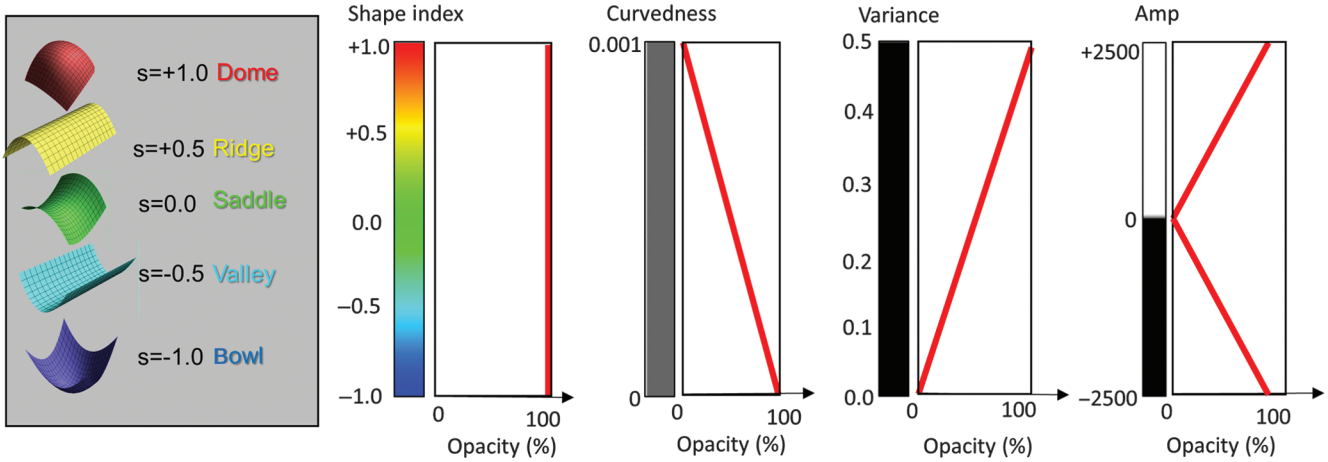

Figure 14. Vertical slices and time slice at $t = 1.226$ s through the shape index plotted against hue and curvedness plotted against saturation. Seismic amplitude is plotted on the vertical slice, and variance is plotted on the time slice. The cartoon to the left of the shape index color bar identifies end-member shapes at −1.0 (a bowl), −0.5 (a valley), 0.0 (a saddle), +0.5 (a ridge), and +1.0 (a dome). The shape for nearly planar (low values of curvedness) structures is poorly defined and appears as uniform gray using our HLS color scheme. Note the ridge (yellow) and valley (cyan) lineaments bracketing the two faults corresponding to conjugate faults comprising a larger damaged zone. Karst collapse features have a bowl shape and appear as blue.

curvatures on the background image shown previously in Figure 6. In this manner, we note that the red, anticlinal, or domal features seen in the curvature correlate directly to those features seen in the vertical seismic amplitude section.

In Figure 9, I use a variation of the same technique to corender an energy attribute (the energy of a Karhunen-Loeve filtered or "coherent" part of the data in a 3-trace × 3-trace × 11-sample analysis window) with its gradient along structural dip and azimuth. This attribute is not available in Petrel but was computed using a separate software package. Barnes (2011) computes a similar attribute by computing the horizontal derivatives of the envelope of the analytic trace. Here, I plot the energy gradients against a binary black and white color bar, using transparency to make the image more black (or white) as I approach strong negative (positive) values of the gradient. Because I am using transparency, white does not show up well against a white background, such that I set the background of Figure 9b and 9c to be gray (with lightness = 50%, or in Petrel, LUM = 120 out of 240). Note the result appears similar to a shaded relief image, but of energy rather than elevation. The channels in the north-central part of the image are nicely delineated as is the bright-red structural high that forms the base of an angular unconformity that is being drained by these channels.

Dip azimuth modulated by dip magnitude

With these simple concepts, I can now simulate the HLS color model in Petrel. Figure 10 shows the same time slice and vertical slices shown in Figure 6, but now through a dip azimuth volume. Dip azimuth and dip magnitude were computed using Petrel's "consistent dip" algorithm (Aarre, 2010). Note the artifacts in Figure 10a. My survey contains 600 inlines and 660

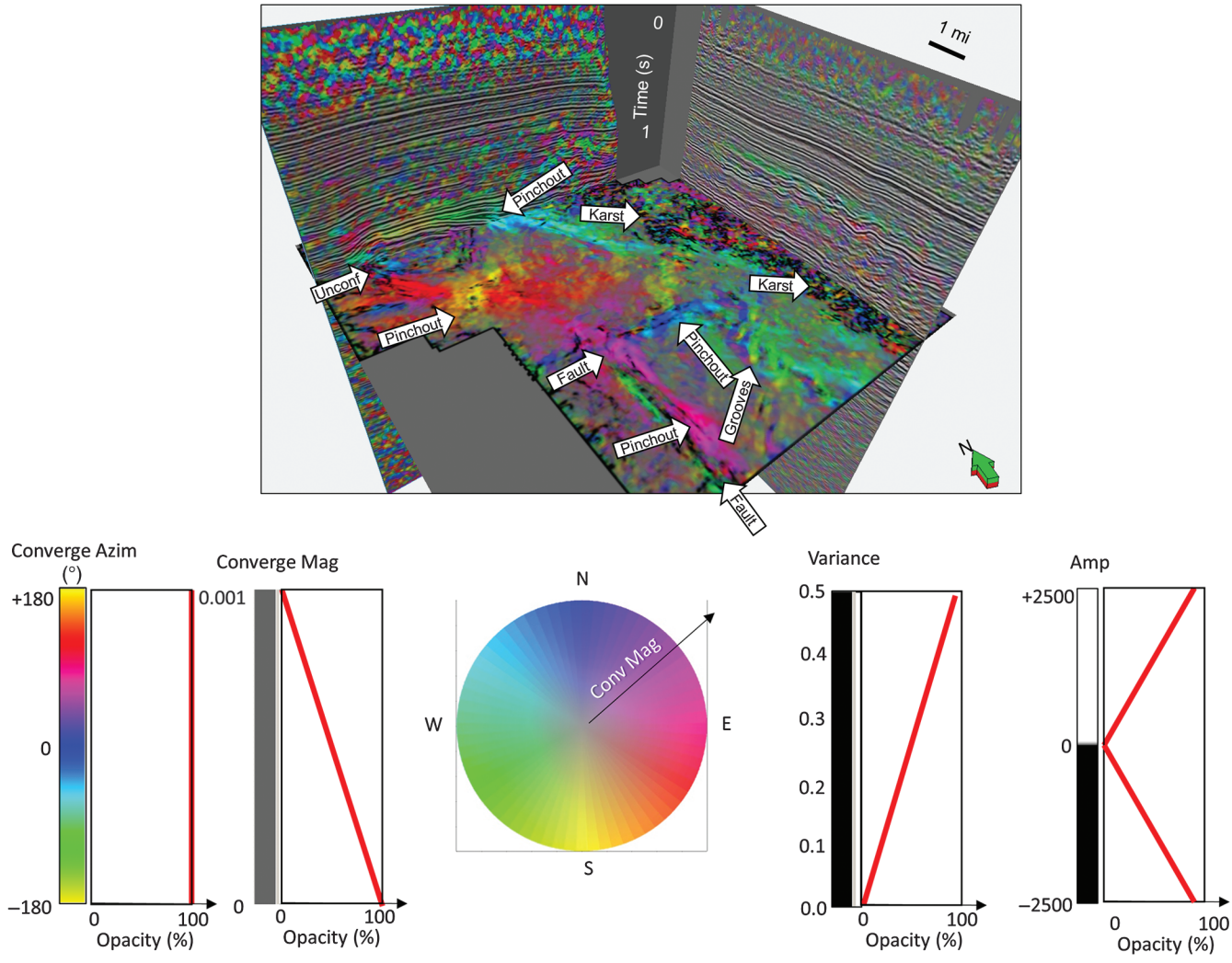

Figure 15. Vertical slices and a time slice at $t = 1.150$ s through the azimuth of reflector convergence plotted against hue as the background corendered with the magnitude of reflector convergence plotted against saturation. Seismic amplitude plotted on the vertical slice, and variance plotted on the time slice against lightness. Note the west–northwest-trending pinch out seen in cyan on the vertical slice that can be traced across the time slice.

crosslines but is displayed using a monitor that is 1800 × 1240 pixels, requiring interpolation. The default in Petrel (and almost every software package I have used) is to smoothly interpolate the values from adjacent voxels. Careful inspection of the color bar in Figure 10 will show that if the voxel to the left has an azimuth of −170° (yellow) and the voxel to the right has an azimuth of +170° (also yellow), the interpolate value will be 0° (or blue). I have captured the "interpolation method" box in Petrel's "settings" file in the lower right. By changing from "smooth" to "none" (which displays the value of the nearest neighbor) for interpolation, I obtain the artifact-free image shown in Figure 10b. This display "feature" is common to all workstation software, and it needs to be addressed for any cyclical color bar: phase, azimuth, or strike.

Figure 11 summarizes the color bars I use for HLS display. I use a cyclical color bar (Figure 11a) for dip azimuth and set it to be 100% opaque as the background. I use a monochrome gray color bar (S = 0%, L = 50%, H = anything) and 100% opacity for flat dip and 0% opacity (100% transparent) for steep dip . The maximum dip of 5° in Petrel's consistent dip (Aarre, 2010) is computed using a time to depth conversion velocity of 2000 m/s, and as such it should be considered to be a relative dip magnitude. The exact values of HLS and RGB for these colors in Petrel are defined in Appendix A.

Variance is Petrel's version of the generic coherence attribute, computed accurately along structural dip. Variance is large in the presence of discontinuities and small when the reflectors have a good signal-to-

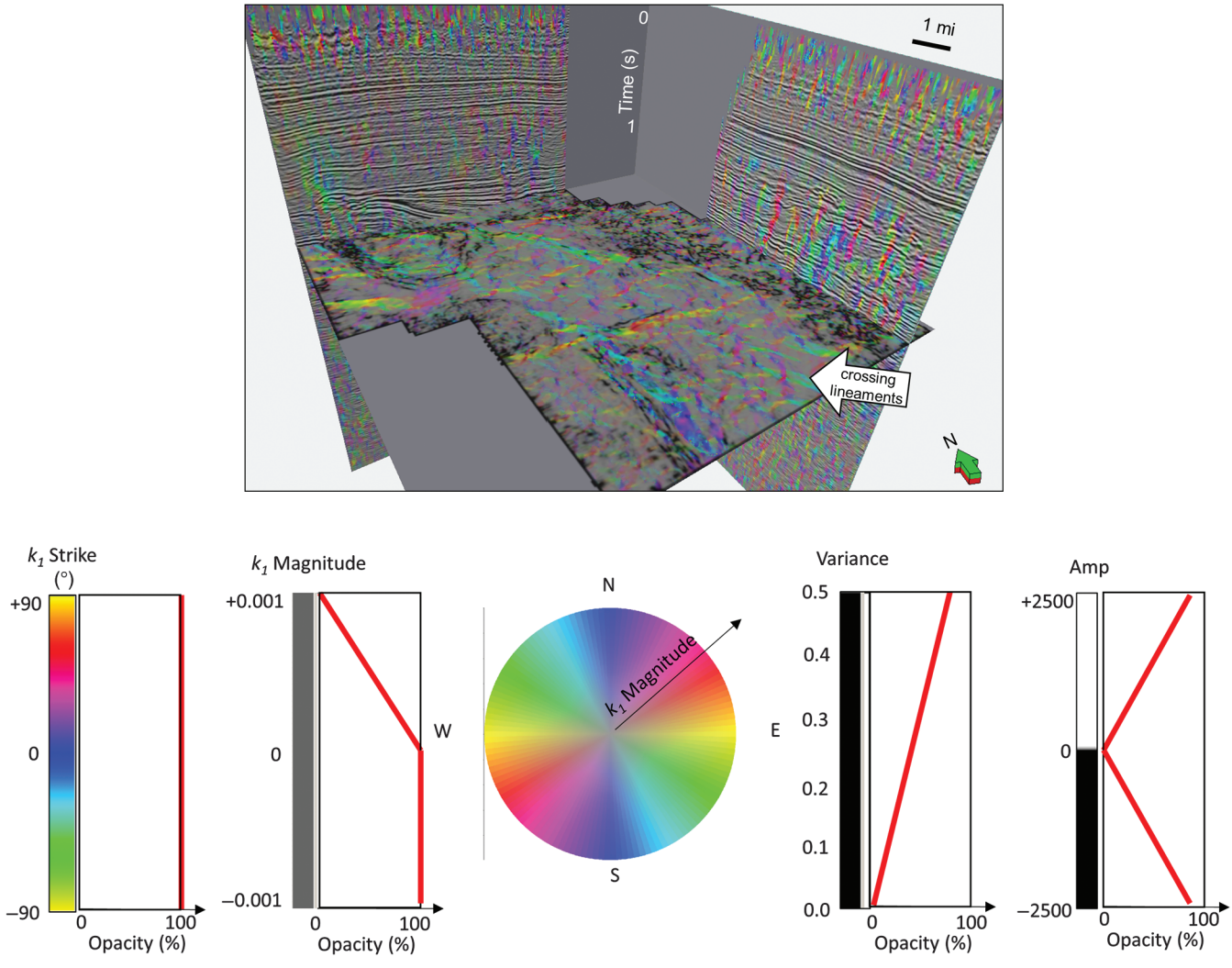

Figure 16. Vertical slices and a time slice at $t = 1.226$ s through the strike of the most-positive curvature plotted against hue as the background corendered with the magnitude of most-positive curvature plotted against saturation. Note that a strike of −90° is displayed the same as a strike of +90°. Seismic amplitude is plotted on the vertical slice, and variance is plotted on the time slice against lightness. Although color coding the curvature lineaments by their strike allows one to see that they are crossing (white arrow), most interpreters would also see this pattern in the simpler, dual-gradational color bar rendering of most-positive curvature used in Figure 8. The true value of strike is in the correlation of hypothesized open fractures to production, where different fracture sets and different diagenetic history may be correlated to azimuthally limited lineaments (e.g., Guo et al., 2011).

noise ratio (S/N) and are continuous. Because I want to "see" the value of dip azimuth versus dip magnitude for the coherent reflectors, I construct the color bar shown in Figure 11d. High-variance (low-coherence) values will be opaque black. Zero-variance values will be transparent. Moderately large values of variance will appear as midnight colors, providing a degree of confidence in our dip computations. In general, areas of low variance result in accurate estimates of reflector dip, such that areas of high variance mask those dip estimates that are less accurate. Such corendering is useful for other attributes such as impedance inversion that assumes locally planar reflectors.

Finally, I will display seismic amplitude as a binary black-and-white color bar using the bilinear opacity curve shown in Figure 11e enabling me to "see through" low-amplitude values. I do not make the extreme amplitude values opaque, but rather I stop at 80%; this value allows me to see the seismic structure on conventional amplitude data without masking the dip information below.

Figure 12 shows the horizontal and vertical slices displayed in Figure 10b, but now corendered with dip magnitude using the color bar in Figure 11b, simulating an HS color model. Figure 13 shows the same slices but now also corendered with variance on the time slice using the color bar in Figure 11d and with amplitude on the vertical slices using the color bar in Figure 11e, simulating an HLS color bar.

Shape index modulated by curvedness

The shape index s and curvedness C (e.g., al-Dossary and Marfurt, 2006) provide an alternative means of displaying the most-positive and most-negative principal curvatures, k_1 and k_2, displayed in Figure 8.

The legend of Figure 14 shows that specific values of the shape index s correspond to bowl, valley, saddle, ridge, and dome shapes. If the curvedness, $C = 0$, the "shapes" degenerate into a plane. As in Figure 12, where the dip-magnitude modulates the dip-azimuth, in Figure 14, curvedness modulates the shape index. When the shape index becomes poorly defined as the curved-

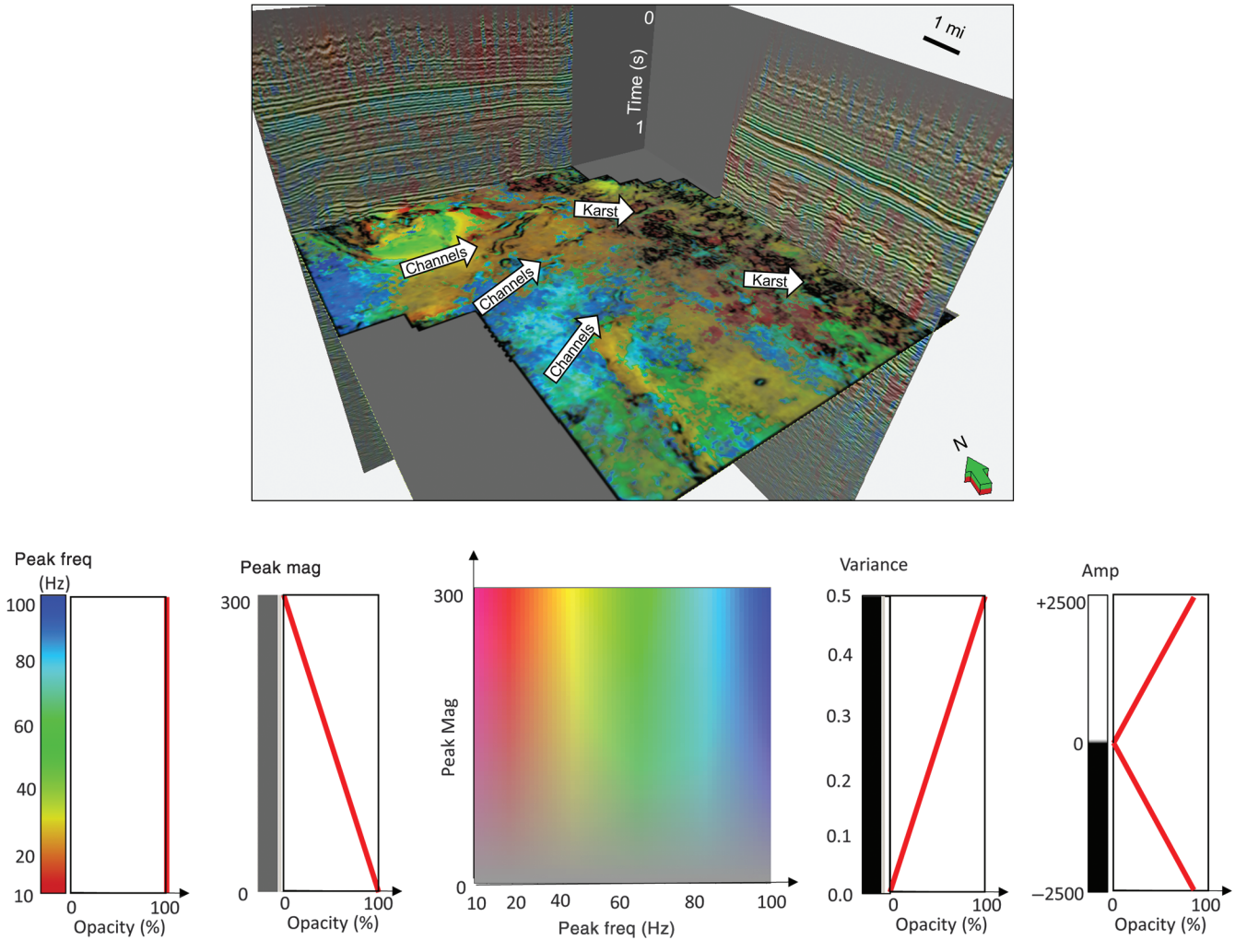

Figure 17. Vertical slices and a time slice at $t = 1.060$ s through peak spectral frequency plotted against hue corendered with peak magnitude plotted against saturation. Seismic amplitude corendered on the vertical slice using a binary black-and-white color bar and variance plotted on the time slice against lightness. The tuning frequency can be read directly from the color bar.

ness approaches zero, the image becomes progressively grayer, regardless of the shape. Figure 14 shows the same fault bracketing by ridges and valleys as seen in Figure 8. The karst also appears as deep blue bowls, surrounded by incoherent (high variance) rims.

The azimuth of reflector convergence modulated by the magnitude of reflector convergence

The 2D displays of reflector convergence are first introduced by Barnes (2000), whereas reflector parallelism is a common workstation seismic attribute. Like dip azimuth and dip magnitude, 3D reflector convergence (Marfurt and Rich, 2010) in Figure 15 is represented by an azimuth (plotted against hue) and a magnitude (plotted against saturation). Note the Pennsylvanian-age angular unconformity at approximately $t = 1.0$ s in the background vertical seismic section where later sediments truncate against the previous structure. Red areas on the time slice at $t = 1.150$ s indicate convergence (pinching out) to the southeast, cyan to the northwest, magenta to the northeast, blue to the north, and yellow to the south. The karsted area on the east side of the data shows very complicated convergence patterns as overlying sediments drape into the karst collapse features. The gray color indicates parallel reflectors (flat or dipping) that can be validated on the two vertical slices. The shallow section ($t < 0.4$ s) seen on the vertical slices has low S/N due to stretch mutes and subsequent low fold, giving rise to inaccurate estimates of dip.

The strike of most-positive curvature modulated by its magnitude

Mathematically, the maximum curvature, is computed as the first eigenvalue-eigenvector pair ($k_{\max}$, $\varphi_{\max}$) that represents the variation of a deformed 2D surface. The minimum curvature is computed as the second eigenvalue-eigenvector pair ($k_{\min}$, $\varphi_{\min}$), where the eigenvectors are perpendicular to each other in the plane tangent to the surface location being analyzed. By the definition of eigenvalues, $|k_{\max}| \geq |k_{\min}|$. Because $k_{\max}$ and $k_{\min}$ can change sign rapidly, I like to use the most-positive and most-negative principal curvatures k_1 and k_2 that are defined as $k_1 = \mathrm{MAX}(k_{\min}, k_{\max})$ and $k_2 = \mathrm{MIN}(k_{\min}, k_{\max})$. Furthermore, I prefer to add 90° (in the dipping plane) to

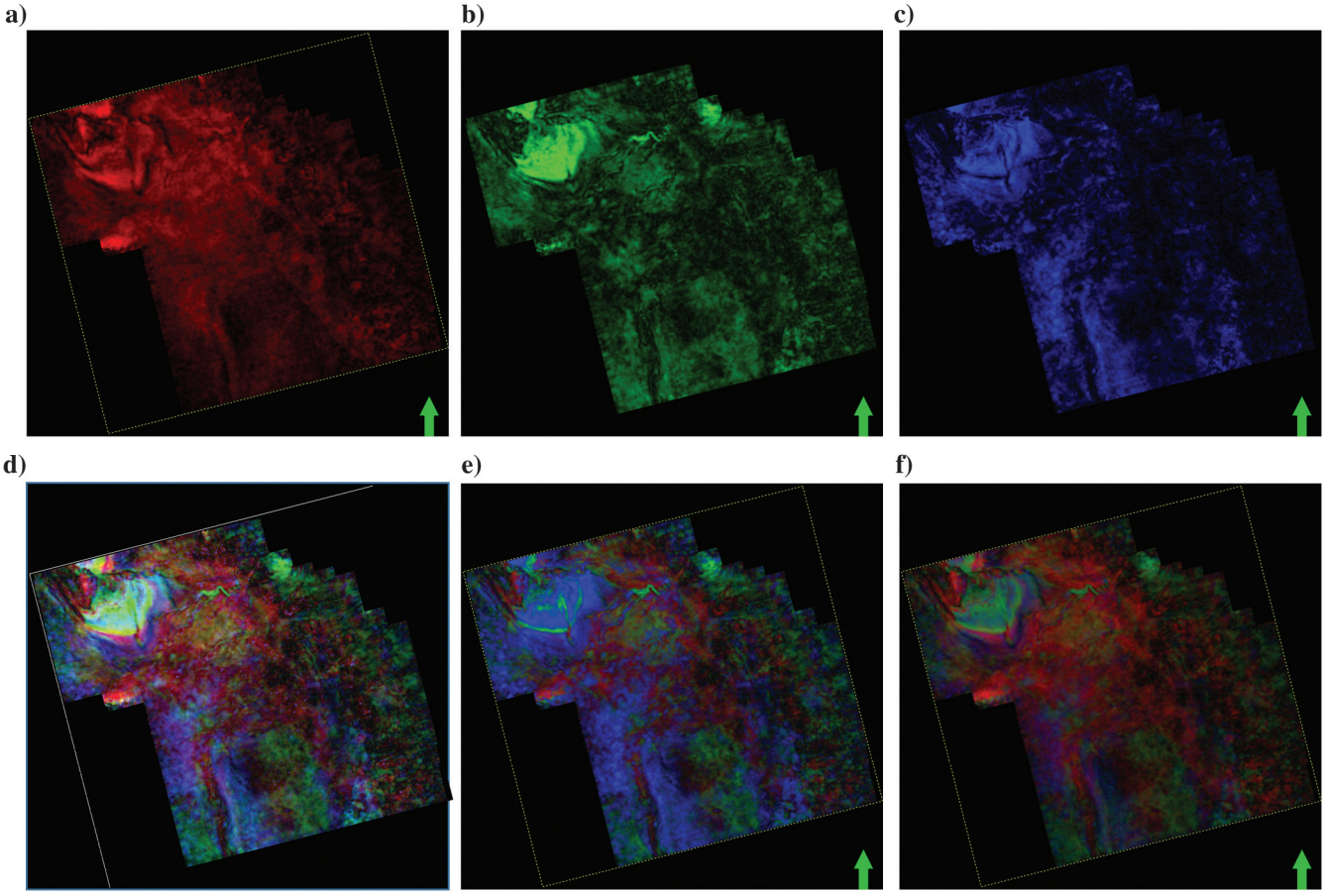

Figure 18. Time slices at $t = 1.060$ s through spectral magnitude components at (a) 20 Hz plotted against red, (b) 40 Hz plotted against green, and (c) 60 Hz plotted against blue. (d) The desired image obtained by color addition of the RGB components shown in panels (a-c) using external software. (e) Corendering where the opacity ranges from 0.0 to 1.0 for each component. Note the last (blue) image overprints the previous images. (f) Corendering a maximum opacity of $(1 - \alpha) = 1/2$ for panel (b) and a maximum opacity of $(1 - \beta) = 1/3$ in panel (c). The color blending works correctly in terms of the hue, but the lightness can never be greater than 33%, resulting in a more muted, grayer image than the desired bright image seen in panel (d).

convert the azimuth of maximum and minimum curvature φ_{max} *and* φ_{min} to be strikes ψ_1 and ψ_2 projected onto the horizontal plane. Figure 16 modulates the strike of the most-positive curvature, ψ_1, plotted against hue by the value of the most-positive curvature k_1 plotted against saturation. These images allow the visualization of the network of positive folds and flexures, in this example, corendered with variance.

Peak spectral frequency modulated by peak spectral magnitude

Time-variant spectral analysis provides a great deal of insight into seismic data, but at the expense of a multitude of spectral magnitude and phase volumes. Because the peak frequency of a spectrally balanced seismic data volume can often be correlated to the temporal tuning thickness, it is, along with spectral bandwidth, one of several attributes that summarize the spectral statistics. Obviously, an estimate of tuning thickness from peak frequency for areas of anomalously low reflectivity are less meaningful than estimates from areas of high reflectivity. Figure 17 modulates the peak frequency plotted against hue by the peak magnitude plotted against saturation. Areas of low reflectivity appear as grayer shades, whereas variance clearly delineates the channel edges and karst collapse features. The previous examples show in how two attributes form components of a vector, while in others that a second attribute provides a level of confidence in the first. Table 1 summarizes some of these display pairs/triplets, while Table 2 shows how pairs of attributes can be plotted against each other using a conversion from Cartesian to polar coordinates.

Red-green-blue color blending versus red-green-blue color addition

A common way to represent spectral components is to blend three components against the RGB color bars

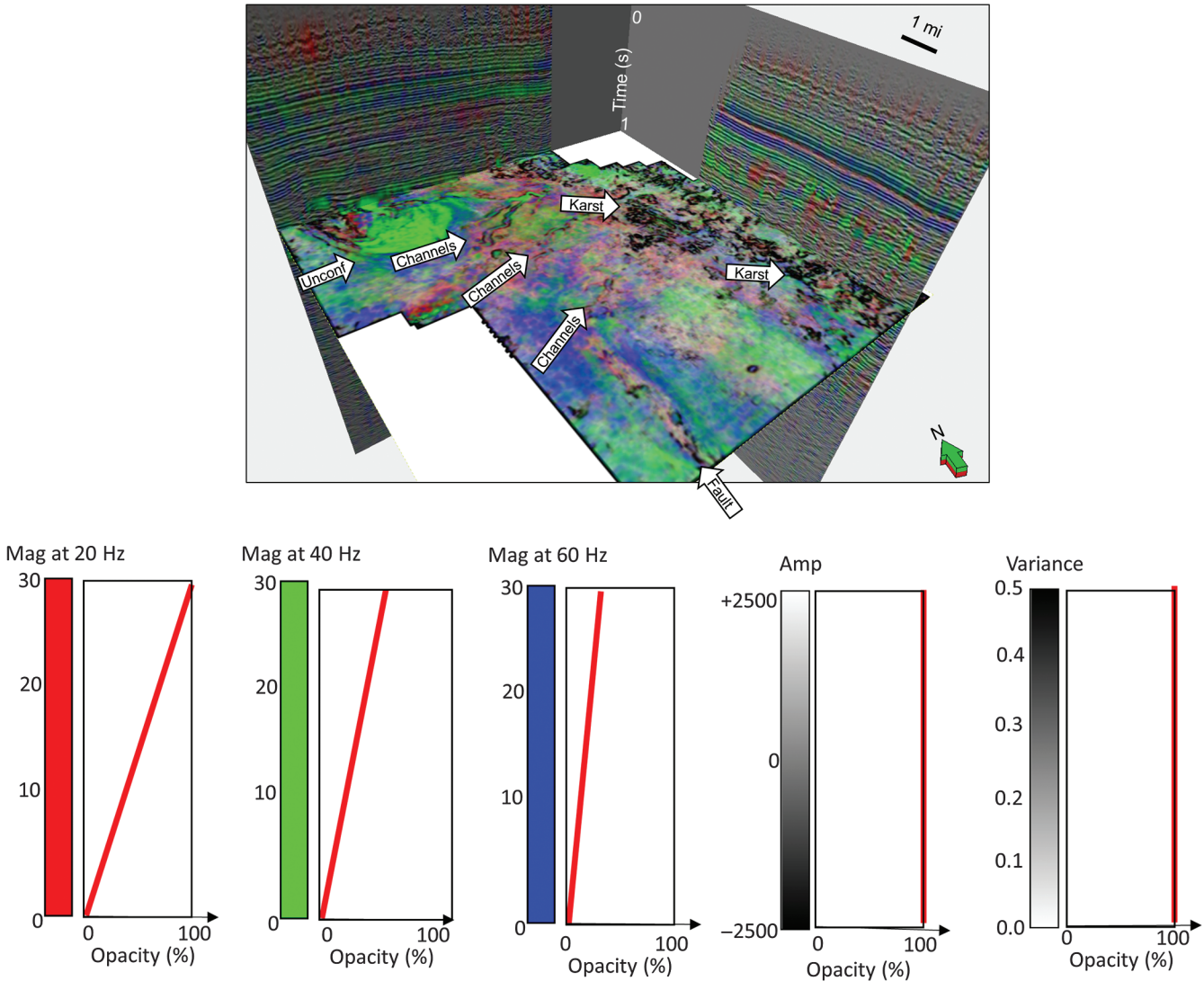

Figure 19. Vertical slices and a time slice at $t = 1.060$ s through 20-, 40-, and 60-Hz spectral components plotted using the RGB color bars shown below. Seismic amplitude is plotted on the vertical slice, and variance is plotted on the time slice forming 100% opaque backgrounds. Note the tuned channels.

and add them, much as occurs on your color television or computer monitor. Figure 18a–18c shows three time slices at $t = 1.060$ s through the 20- (plotted against red), 40- (plotted against green), and 60-Hz (plotted against blue) spectral magnitude components. For simplicity, the background was set to black. Many commercial software packages provide simple addition of these color bars to obtain an image such as that shown in Figure 18d. If all three spectral components reach their peak value (or are clipped), they should appear as white using the RGB color model in Figure 1a. The commercial software package I use does not yet have this capability. Although corendering two attributes against a monochrome gray and black color bar simulates the HLS color model (shown in Figure 1b), this same "trick" does not work for monochromatic RGB color bars. Allowing the maximum values of $\alpha = 1$ and $\beta = 1$ in equation 3 results in Figure 18e, in which the last blended attribute, the 60-Hz magnitude component plotted against blue, overprints rather than adds to the previously displayed red and green images. The best compromise is to set $\alpha = 1/2$ and $\beta = 1/3$, such that if the values of each of the three components reach or are clipped to the maximum value at a given voxel, they will be displayed as a shade of gray with 33% lightness. Figure 19 shows an RGB image that correlates well to that shown in Figure 17 using peak frequency and peak magnitude. In this example, variance was corendered using the lightness axis. Simulating CMY, or color subtraction, such as presented by Purves and Basford (2011) is similarly limited.

These limitations are less important when using Petrel 2014's "box" probe or "surface" probe. In these two cases, one wishes to visualize and then optically stack a suite of planes or surfaces at the same time. Obviously, to see through the nearest slice or surface, one needs to

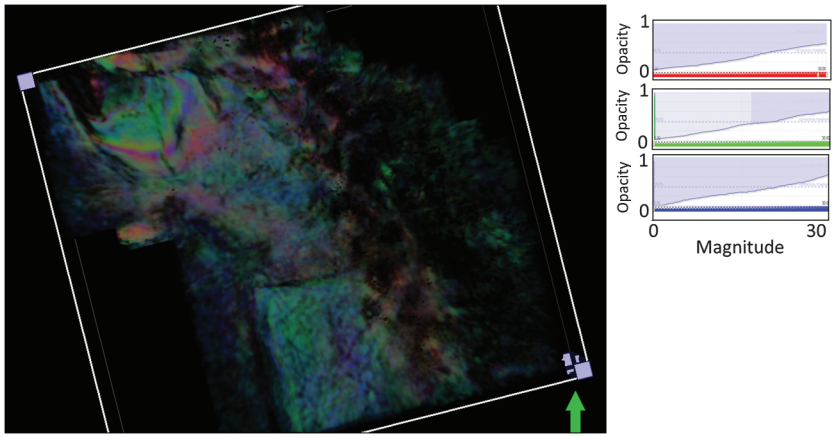

Figure 20. RGB color blending using Petrel's "box probe" tool. The thickness of this window is about 50 ms or 26 samples. Blending occurs differently in this tool, with equal opacity curves, shown in the legend ranging from 0.0 for zero magnitude to 0.6 for the clipped magnitude, providing the correct tuning images. As with Figure 19, an opacity of 1.0 for all three images does not generate white, but a gray level with lightness = 1/3.

Table 1. A partial list of attributes that can be effectively displayed against an HLS color model.

Background attribute (against hue)	Modulating attribute (against saturation)	Calibration attribute (against lightness)	Reference
Dip azimuth	Dip magnitude	Coherence on time slices. Amplitude on vertical slices.	Figure 12, Rijks and Jauffred (1991), Marfurt et al. (1998)
Strike of most-positive principal curvature	Positive value of most-positive principal curvature	Coherence on time slices. Amplitude on vertical slices.	Figure 16, Guo et al. (2013)
Strike of most-negative principal curvature	Positive value of most-negative principal curvature	Coherence on time slices. Amplitude on vertical slices.	Marfurt (2010), Guo et al. (2010)
Reflector shape index	Reflector curvedness	Coherence on time slices. Amplitude on vertical slices.	Figure 14, Mai et al. (2009), Marfurt (2010)
Peak spectral frequency	Peak spectral magnitude	Coherence on time slices. Amplitude on vertical slices.	Figure 17, Guo et al. (2008)
Azimuth of reflector convergence	Magnitude of reflector convergence	Coherence on time slices. Amplitude on vertical slices.	Figure 15, Marfurt (2010), Marfurt and Rich (2010), Chopra and Marfurt (2011)
Azimuth of HTI anisotropy	Magnitude of HTI anisotropy	Confidence of fit, coherence, most-positive curvature, most-negative curvature on time slices. Amplitude on vertical slices.	Guo et al. (2010), Zhang et al. (2013)
Azimuth of vector correlation	Magnitude of vector correlation	Coherence on time slice. Amplitude on vertical slices.	Guo et al. (2013)
Most likely facies number	None	Probability of facies	Espersen et al. (2000)

Table 2. A partial list of attributes that can be plotted against the *x*- and *y*-axes, converted to radial coordinates to generate an azimuth and magnitude centered in the 2D histogram. The azimuthal component is then plotted against hue, and the radial component is plotted against either lightness or saturation.

x-axis	*y*-axis	Calibration attribute (against lightness)	Reference
Lambda-rho	Mu-rho	Coherence on time slices. Amplitude on vertical slices. Microseismic events as icons.	Perez and Marfurt (2013)
Latent space axis 1	Latent space axis 2	Coherence on time slices. Amplitude on vertical slices.	Strecker and Uden (2002), Wallet et al. (2009), Roy et al. (2011)

set the opacity to be less than 1.0 for the peak values. I find that setting the opacity to be 0.6 at the maximum magnitude provides a good image (Figure 20). Setting the opacity to be 1.0 results in gray with a lightness of 1/3 rather than white, indicating that the RGB values do not add.

Conclusions

Many attributes, including dip azimuth-dip magnitude, curvature strike-curvature magnitude, reflector convergence azimuth-convergence magnitude, and strike of maximum P wave velocity-magnitude of P wave velocity azimuthal anisotropy, form components of a vector and are best plotted together using radial coordinates mapped against a hue-lightness or HS 2D color model. Other attributes form natural pairs, such as phase vs. envelope, shape index vs. curvedness, peak frequency vs. peak magnitude, impedance vs. rms data misfit error, and lithology vs. type confidence in classification, in which the second member provides a measure of confidence or reliability. Still other attribute pairs such as $\lambda\rho - \mu\rho$ and SOM or GTM latent spaces can be plotted against 2D color bars. All of these 2D images can be further modulated by lightness, using attributes such as coherence, seismic amplitude, or confidence of a dip, cluster, or inversion estimate.

By corendering or modulating the second and third attributes against monochrome gray and black, gray and white, or gray and binary black-and-white color bars, one can accurately simulate an HLS color model. Although I have demonstrated this trick/technique in Petrel 2014, it will work similarly in any 3D visualization software package that provides alpha-blending capabilities (commonly called *transparency* or *opacity*). The blending technique works well even with only 256 definable colors for a given attribute, with blending effectively rendering $(256)^3$ colors. Furthermore, although I have exclusively shown piecewise constant or linear blending curves for simplicity, the interpreter can accentuate or attenuate any feature of interest by interactively modifying the blending (transparency/opacity) coefficients α and β.

Unfortunately, this technique is less satisfying for RGB color addition and CMY color subtraction. However, when attempting to do so, it is appropriate to use monochrome RGB color bars, with blending of $\alpha = 1/2$ and $\beta = 1/3$, and not black-to-red, black-to-green, and black-to-blue color bars with equal blending that I see many of my colleagues use.

Blending works well with three attributes. Overprinting a "sparse" edge-sensitive attribute such as coherence on an RGB spectral component image can extend the number to four attributes in some instances. I suspect that this limitation is correlated to human visual physiology of (three-color receptor) cones and (lightness) rods. If we had the four-color receptors of birds, we could plot a fourth attribute against ultraviolet.

Acknowledgments

I generated my first three-attribute display using Uniras software in the mid-1980s. Since that time, I have wanted to generate interactive HLS plots in commercial visualization software available to me, but I could never figure out how to do so. Thanks to M. Hedefa and participants in a short course held in Saudi Aramco during spring 2014 for providing the correct environment to figure this out. The combination of an overstimulated mind, hands-on access to Petrel, engaged class participants, serious jet lag, and sleepless nights resulted in these workflows.

The license to the seismic data was provided courtesy of Burlington Resources as part of a Department of Energy study on carbonates and CO_2 sequestration. The variance, dip azimuth, dip magnitude volumes, and all displays were made in Petrel 2014. Thanks go to Schlumberger for providing licenses to the University of Oklahoma (OU) for use in research and education. Other attributes were generated using OU attribute assisted seismic processing and interpretation software. Thanks go to A. Barnes, V. Aarre, and an anonymous reviewer for constructive criticism and suggestions that improved this paper.

Appendix A

Constructing color bars and corendering multiple attributes in Petrel

The body of this paper is written to be quite generic, including the "interpolation" issue addressed in Figure 10, and is common to most commercial interpretation packages. As mentioned in the preface, several commercial packages provide direct display of attrib-

utes against the HLS color model, and several provide RGB color addition and CMY subtraction. This appendix is written for those using Petrel 2014. I expect this appendix to be outdated within a few years, so I will keep it short.

Constructing color bars in Petrel 2014

Petrel 2014 supports color definition using either an RGB or HLS model (Figure A-1). RGB ranges between zero and 255, H ranges between zero and 239, and L and S range between zero and 240. The color selection tool displays a 2D H versus S color model (with fixed L = 120) (Figure A-1a). A second color bar shows the chosen color plotted against L (Figure A-1b). The chosen color is displayed with HLS and RGB numerical value components. Modifying the components in one color model is interactively converted to the second (Figure A-1c). Figure A-2a shows the variation of red (H = 0) along the lightness axis for a fixed saturation = 240, and Figure A-2b shows the variation of red along the saturation axis for a fixed lightness = 120.

Familiarity with the above color model allows one to define the cyclical color bar shown in Figure A-3. Colors can be interpolated linearly in RGB space and either clockwise or counterclockwise in HLS space. Setting both extremes of the color bar to be the same value (in this case, blue), prevents the software from flipping the polarity of the color bar to set red to +60°. Rather, choosing colors that are closely spaced (e.g., 160 and 159) provides greater flexibility, allowing one to flip the direction. In my work, I use the same range of colors, i.e., blue for 0° phase and blue for 0° azimuth or strike for all the cyclical attributes. The default in Petrel is to have a color range of magenta to magenta for azimuths of 0° – 360° and phases of −180° to +180°, such that 0° azimuth appears as magenta but 0° phase appears as green. Modifying the color bars to be consistent avoids subliminal interpretation mistakes.

Corendering attribute slices in Petrel 2014

Corendering vertical and time slices in Petrel 2014 is simple. However, my experience in teaching short courses is that this feature is underused, perhaps because the interpreters do not know why they may wish to use it (the purpose of this tutorial), or perhaps because the key toggle button is easily overlooked and the sequence of events to activate the linkage is quite specific. I summarize this sequence of button clicks in Figure A-4. Once linked together, each of these slices can be dragged to different locations while maintaining the overlay. Sometimes, an interpreter will wish to assign two different color bars to the same volume, for example, plotting seismic amplitude against an opaque cyan-blue-white-red-yellow color bar for amplitude analysis and the black-and-white bimodal color bar shown in Figure 11e for overlays. In this case, rather than copying the volume one inserts a new "virtual" volume and assigns it the appropriate color bar.

Loading and displaying 2D color tables

Figure A-5 shows common pitfalls associated with loading 2D color tables as a multiplexed 1D color bar, as described by Guo et al. (2008). Many commercial software packages do not provide a means to load such 2D color tables. Typically, one loads a SEGY format data

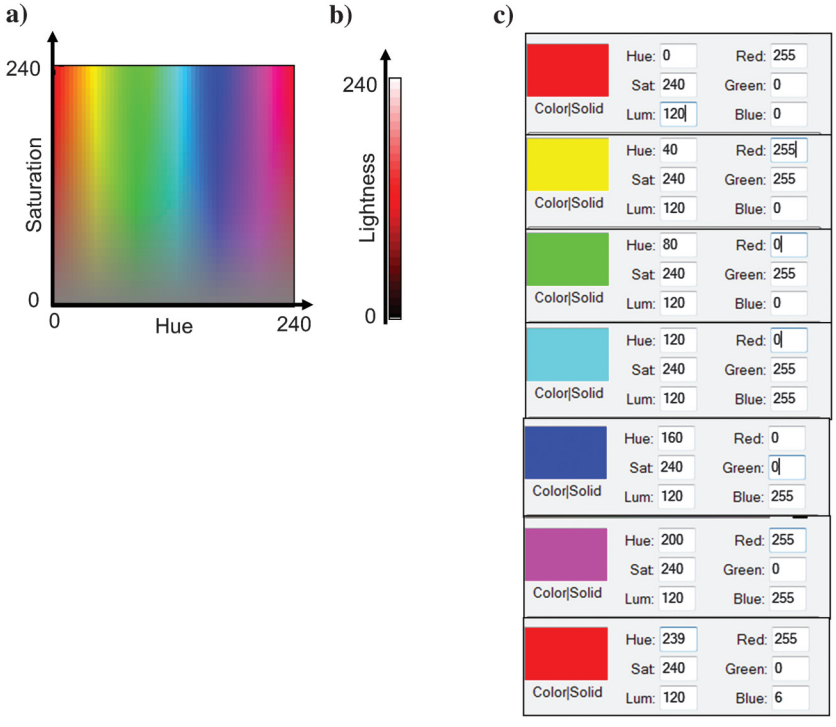

Figure A-1. Elements of the Petrel 2014 color model. The RGB range is between zero and 255. HLS ranges between zero and 240. (a) The 2D HS color bar as it appears in Petrel (with added annotation on the axes). (b) The luminosity (lightness) color axis for hue = 0 (red) and saturation = 240. (c) RGB and CMY colors as shown in Figure 1a. The RGB values are identical, but the HLS values range between zero and 240 rather than the more common zero and 360 for H and 0.0 and 1.0 for L and S. Note that hue = 239 at the bottom is almost red.

volume with values ranging between zero and 255, along with a corresponding 16×16, 256-color table saved as a multiplexed 1D color bar in the appropriate format. Proper data interpolation would be in 2D, not 1D, so to display these images, data interpolation must turned off, as in Figure 10. Unfortunately, there is currently no way to turn off interpolation along surfaces in Petrel 2014, resulting in the image shown in Figure A-5b. Blending the images by simulating the HLS color model described in this paper avoids this limitation, resulting in the correct two-attribute horizon slice shown in Figure A-5d.

A common pitfall: Incorrect graphics card settings

I have seen graphical aliasing on my computers and those of the largest oil companies. If stripes appear on the corendered volumes (for any software), the problem is most likely with the graphics card settings. Typically, the graphics cards come preset to be used for playing computer video games where speed is critical, and graphical precision is less important. Most commercial interpretation software will come with recommended settings for the more popular graphics cards. If encountering graphical aliasing when corendering

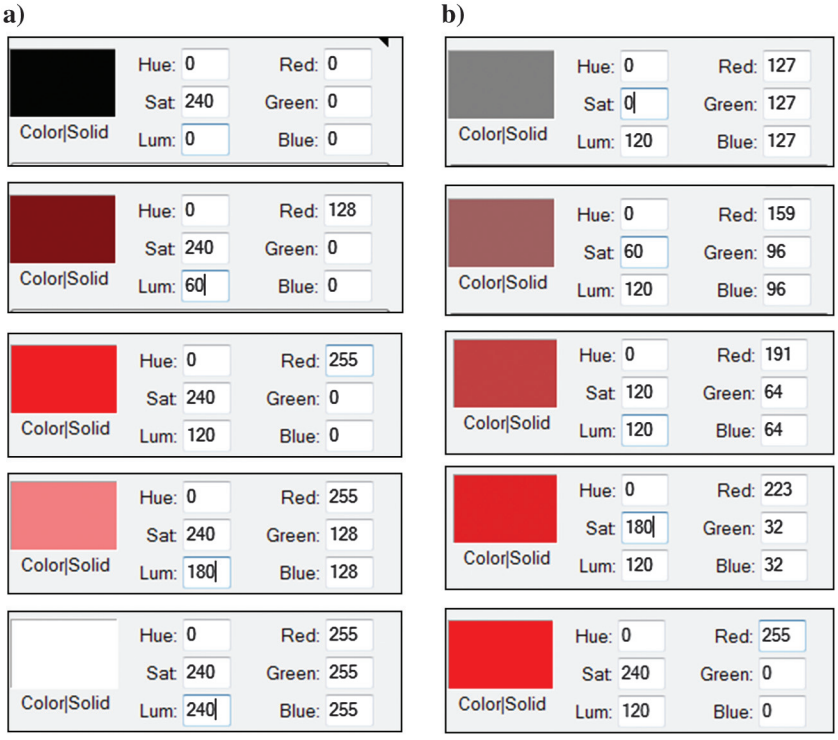

Figure A-2. (a) The luminosity (lightness) axis for hue = 0 (red) and saturation = 240. Colors range from white, through pink, pure red, brick red, to black. (b) The saturation axis for hue = 0 (red) and luminosity ((lightness) = 120. Colors range from gray through progressive shades of dirty red to pure red. Note the mapping from HLS to RGB space for both axes. The trick used in this paper to simulate HLS mapping in Petrel is alpha blending of either black, white, or gray with pure red, as shown in this image.

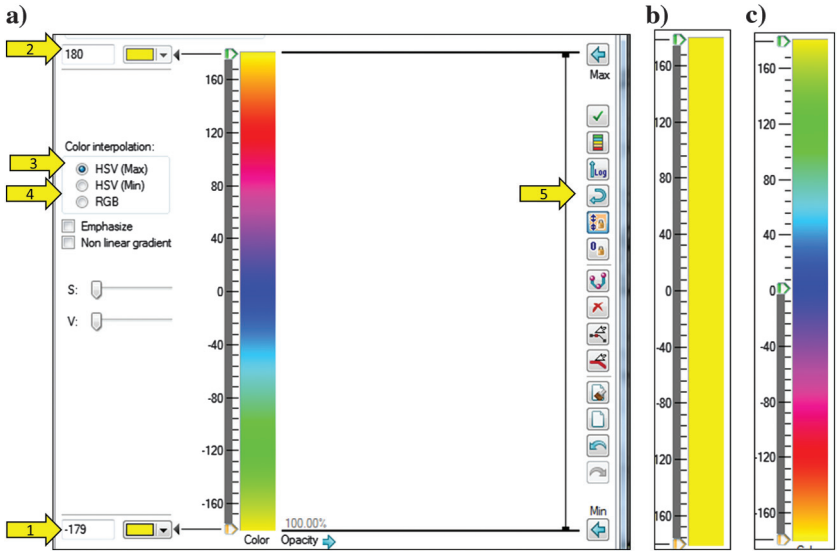

Figure A-3. Generating a cyclical color bar in Petrel. In this case, I want to set both -180° and $+180^{\circ}$ to be yellow. First I click the colors at the bottom and top of the color bar and set them to have Hue = 40(yellow), Sat = 240, and Lum = 120. I then (3) click the HSV (Max) button and obtain the color bar in (a) If I want the cycle to in the opposite direction, and click (4) click the HSV(Min) I get the solid yellow color bar in (b) Instead, I need to explicitly define a blue color at 0°. Then by choosing HSV (Min) in both ranges I obtain the color bar in (c).

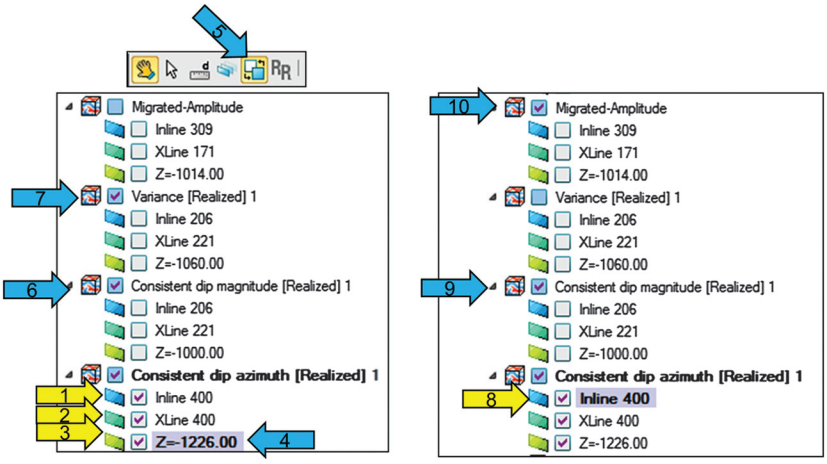

Figure A-4. The first step is to display the background images. In this example, I display (1) inline 400, (2) crossline 400, and (3) a time slice at $t = 1.226$ s through Petrel's consistent dip azimuth volume (Aarre, 2010) using the color bar and opacity shown in Figure 11a to obtain the image shown in Figure 10. Next, I (4) highlight the first plane to be corendered and (5) click the "visualize on intersection" blue/white square button adjacent to the "manipulate plane" icon. When the blue/white button is toggled, the boxes in front of the various seismic data volumes turns blue or white. When they are blue, place a check mark in front of (6) the consistent dip magnitude volume using the color bar shown in Figure 11b and obtain the time slice shown in Figure 12. Next, (7) place a check mark in front of Petrel's variance volume using the color bar shown in Figure 11d and obtain the time slice shown in Figure 13. Repeat this process by highlighting (8) inline 400 through the dip azimuth volume and (toggling to turn the boxes in front of volumes blue if necessary) placing a check mark in front of the (9) consistent dip magnitude volume and (10) migrated seismic amplitude volume, the latter of which uses the color bar shown in Figure 11e. Repeating this process for crossline 400 results in the three corendered slices shown in Figure 13. These three slices are now linked and can be moved interactively. To unlink a given attribute, highlight the slice of interest and remove the check mark in blue box.

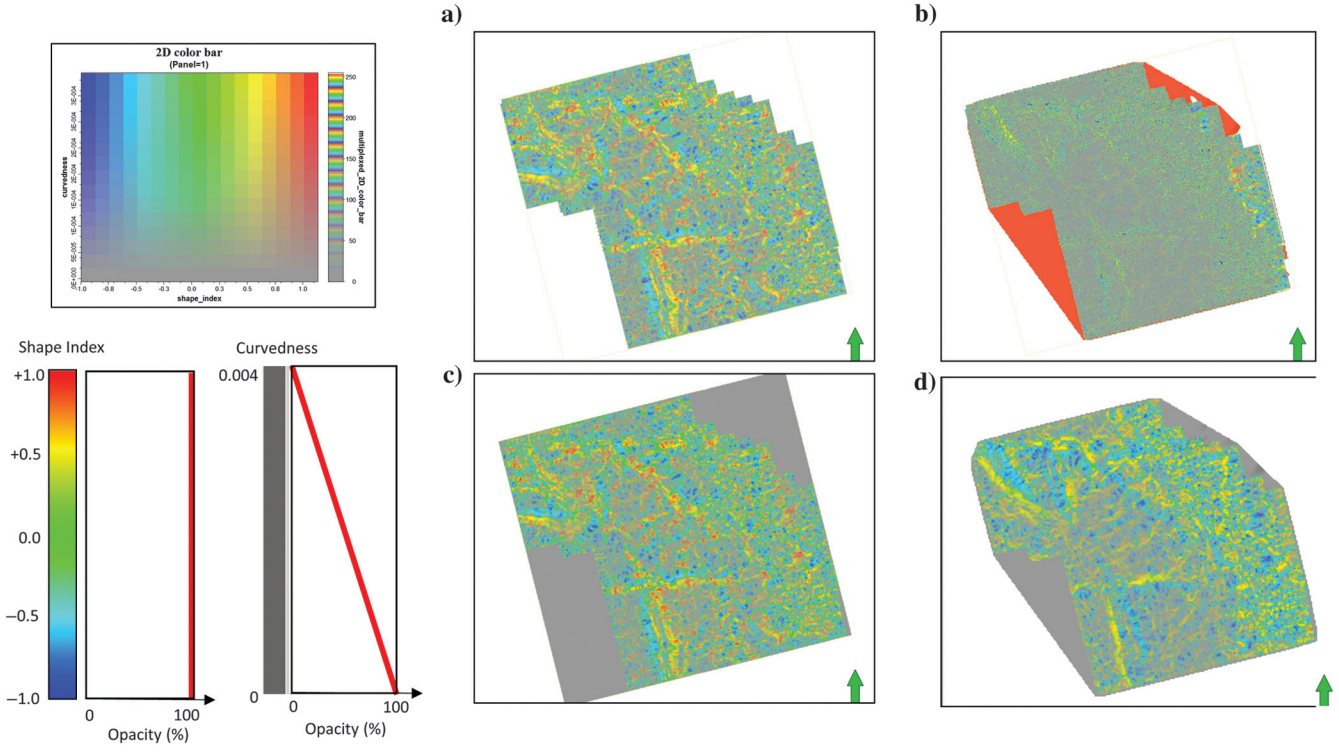

Figure A-5. Comparison of color modulation using an (a) explicit and (b) 16 × 16 2D color table containing 256 colors and (c and d) using two 1D color bars and opacity. With the exception of the zero-valued traces outside the survey limits, the two times slices (a and c) at $t = 1.226$ s are almost identical. Interpolation has been turned off. However, there is no option to turn off interpolation on horizon slices such that the horizon slice at the Atoka level is aliased when using a 2D color bar. There is no aliasing when corendering the images using the two 1D color bars and opacity in panel (d).

and the workstation is using a supported graphics card, the graphics card default settings may need to be reset on the control panel (for Windows-based software). One then needs to choose the settings either for the specific interpretation software package or for a generic computer-aided design and manufacturing software (CAD/CAM) application.

References

Aarre, V., 2010, Globally consistent dip estimation: 80th Annual International Meeting, SEG, Expanded Abstracts, 1387–1391.

Al-Dossary, S., and K. J. Marfurt, 2006, Multispectral estimates of reflector curvature and rotation: Geophysics, **71**, no. 5, P41–P51, doi: 10.1190/1.2242449.

Balch, A. H., 1971, Color sonograms: A new dimension in seismic data interpretation: Geophysics, **36**, 1074–1098, doi: 10.1190/1.1440233.

Barnes, A. E., 2000, Attributes for automated seismic facies analysis: 70th Annual International Meeting, SEG, Expanded Abstracts, 553–556.

Barnes, A. E., 2002, What a relief shade can be: AAPG Explorer, **8**, http://www.aapg.org/explorer/geophysical_corner/2002/08gpc.cfm, accessed 22 June 2005.

Barnes, A. E., 2007, Redundant and useless attributes: Geophysics, **72**, no. 3, P33–P38, doi: 10.1190/1.2716717.

Barnes, A. E., 2011, Displaying seismic data to look like geology: Presented at GCSSEPM 31st Annual Bob. F. Perkins Research Conference on Seismic attributes — New views on seismic imaging: Their use in exploration and production, 100–119.

Brown, A. R., 2011, Interpretation of three-dimensional seismic data: AAPG Memoir 42 and SEG, Investigations in Geophysics **9**, 7th ed.

Chopra, S., and K. J. Marfurt, 2007, Curvature attribute applications to 3D surface seismic data: The Leading Edge, **26**, 404–414, doi: 10.1190/1.2723201.

Chopra, S., and K. J. Marfurt, 2011, Which curvature right for you?, GCSSEPM: 31st Annual Bob. F. Perkins Research Conference on seismic attributes, 642–676.

Dao, T., and K. J. Marfurt, 2011, The value of visualization with more than 256 colors: 81st Annual International Meeting, SEG, Expanded Abstracts, 941–944.

Dou, Q., Y. Sun, and C. Sullivan, 2009, Seismic detection of paleocave system and its influence on carbonate reservoir compartmentalization: 69th Annual International Meeting, SEG, Expanded Abstracts, 1731–1735.

Espersen, T. B., T. Veggeland, J. M. Pedersen, and K. B. Rasmussen, 2000, The lithology cube: 70th Annual International Meeting, SEG, Expanded Abstracts, 643–646.

Foley, J. F., and A. van Dam, 1982, Fundamentals of interactive computer graphics: Addison Wesley.

Fu, D., K. J. Marfurt, and E. C. Sullivan, 2006, Attribute analysis of chert reservoirs in the Devonian Thirtyone Formation, West Texas: Geophysics, **71**, no. 5, B151–B158, doi: 10.1190/1.2335636.

Guo, H., S. Lewis, and K. J. Marfurt, 2008, Mapping multiple attributes to three- and four-component color models — A tutorial: Geophysics, **73**, no. 3, W7–W19, doi: 10.1190/1.2903819.

Guo, H., K. J. Marfurt, S. E. Nissen, and E. C. Sullivan, 2010, Visualization and characterization of structural deformation fabric and velocity anisotropy: The Leading Edge, **29**, 654–660, doi: 10.1190/1.3447777.

Guo, S., B. Zhang, T. Lin, and K. J. Marfurt, 2013, Azimuthal AVO gradient anisotropic analysis on prediction of fractures of Barnett Shale: Unconventional Resources Technology Conference, Expanded Abstracts, 1890–1899.

Guo, Y., K. Zhang, and K. J. Marfurt, 2012, Quantitative correlation of fluid flow to curvature attributes: 82nd Annual International Meeting, SEG, Expanded Abstracts, 1–5.

Joblove, G. H., and D. Greenberg, 1978, Color spaces for computer graphics: ACM SIGGRAPH Computer Graphics, **12**, 20–25, doi: 10.1145/800248.807362.

Knobloch, C., 1982, Pitfalls and merits of interpreting color displays of geophysical data: 52nd Annual International Meeting, SEG Expanded Abstracts, 112.

Liner, C., C.-F. Li, A. Gersztenkorn, and J. Smythe, 2004, SPICE: A new general seismic attribute: 72nd Annual International Meeting, SEG, Expanded Abstracts, 433–436.

Liu, J. L., and K. J. Marfurt, 2007a, Instantaneous spectral attributes to detect channels: Geophysics, **72**, no. 2, P23–P31, doi: 10.1190/1.2428268.

Liu, J. L., and K. J. Marfurt, 2007b, Multi-color display of spectral attributes: The Leading Edge, **26**, 268–271, doi: 10.1190/1.2715047.

Lynch, S., J. Townsley, M. Dennis, and C. Gibson, 2005, Enhancing fault visibility using bump mapped seismic attributes: CSEG National Meeting, Expanded Abstracts, http://crewes.org/ForOurSponsors/ConferenceAbstracts/2005/CSEG/Lynch_CSEG_2005.pdf.

Mai, H. T., K. J. Marfurt, and A. S. Chávez-Pérez, 2009, Coherence and volumetric curvatures and their spatial relationship to faults and folds, an example from Chicontepec Basin, Mexico: 79th Annual International Meeting, SEG, Expanded Abstracts, 1063–1067.

Marfurt, K. J., 2010, The shape of seismic interpretation: Presented at GCSSEPM 30th Annual Bob F. Perkins Research Conference on Seismic Geomorphology, 241–294.

Marfurt, K. J., R. L. Kirlin, S. L. Farmer, and M. S. Bahorich, 1998, 3-D seismic attributes using a semblance-based coherency algorithm: Geophysics, **63**, 1150–1165, doi: 10.1190/1.1444415.

Marfurt, K. J., and J. Rich, 2010, Beyond curvature — Volumetric estimation of reflector rotation and convergence: 80th Annual International Meeting, SEG, Expanded Abstracts, 1467–1472.

Masaferro, J. L., R. Bourne, and J.-C. Jauffred, 2003, 3D seismic imaging of carbonate reservoirs and structures: The Leading Edge, **22**, 18–25, doi: 10.1190/1.1542751.

Meyer, D. E., E. L. Harvey, T. E. Bulloch, J. C. Voncannon, and T. M. Sheffield, 2001, Use of seismic attributes in 3D

geovolume interpretation: The Leading Edge, **20**, 1377–1400, doi: 10.1190/1.1486768.

Onstott, G. E., M. M. Backus, C. R. Wilson, and J. D. Phillips, 1984, Color display of offset dependent reflectivity in seismic data: 64th Annual International Meeting, SEG, Expanded Abstracts, 674–675.

Perez, R., and K. J. Marfurt, 2013, Brittleness estimation from seismic measurements in unconventional reservoirs: Application to the Barnett Shale: 83rd International Annual Meeting, SEG, Expanded Abstracts, 2258–2263.

Purves, S., and H. Basford, 2011, Visualizing geological structure with subtractive color blending: Presented at 31st Annual Gulf Coast Section SEPM Foundation Bob F. Perkins Research Conference, 120–139.

Rijks, E. J. H., and J. E. E. M. Jauffred, 1991, Attribute extraction: An important application in any 3-D seismic interpretation: The Leading Edge, **10**, 11–19, doi: 10.1190/1.1436837.

Roy, A., M. Matos, and K. J. Marfurt, 2011, Application of 3D clustering analysis for deep marine seismic facies classification — An example from deep water northern Gulf of Mexico: Presented at GCSSEPM 31st Annual Bob. F. Perkins Research Conference, 410–439.

Strecker, U., and R. Uden, 2002, Data mining of 3D post-stack attribute volumes using Kohonen self-organizing maps: The Leading Edge, **21**, 1032–1037, doi: 10.1190/1.1518442.

Wallet, B. C., M. C. de Matos, J. T. Kwiatkowski, and Y. Suarez, 2009, Latent space modeling of seismic data: An overview: The Leading Edge, **28**, 1454–1459, doi: 10.1190/1.3272700.

Zhang, K., Y. Guo, B. Zhang, A. M. Trumbo, and K. J. Marfurt, 2013, Seismic azimuthal anisotropy after hydraulic fracturing: Interpretation, **1**, no. 2, SB27–SB36, doi: 10.1190/INT-2013-0013.1.

Kurt. J. Marfurt joined The University of Oklahoma in 2007 where he serves as the Frank and Henrietta Schultz Professor of Geophysics within the ConocoPhillips School of Geology and Geophysics. His primary research interest is in the development and calibration of new seismic attributes to aid in seismic processing, seismic interpretation, and reservoir characterization. His recent works focused on applying coherence, spectral decomposition, structure-oriented filtering, and volumetric curvature to mapping fractures and karst with a particular focus on resource plays. He earned a Ph.D. in applied geophysics at Columbia University's Henry Krumb School of Mines in New York in 1978 where he also served as an assistant professor for four years. He worked 18 years in a wide range of research projects at Amoco's Tulsa Research Center after which he joined the University of Houston for eight years as a professor of geophysics and the director of the Allied Geophysics Lab. He has received SEG best paper (for coherence), SEG best presentation (for seismic modeling) and as a coauthor with Satinder Chopra best SEG poster (for curvature), and best AAPG technical presentation. He also served as the EAGE/SEG Distinguished Short Course Instructor in 2006 (on seismic attributes). In addition to teaching and research duties at OU, he leads short courses on attributes for the SEG and AAPG.